photochem

MDPI

Review

Shedding Light on the Proteinaceous Envelope Protecting Luminescent Gold Nanoclusters: A Review

Matylda Wacławska * and Wojciech Dzwolak *

Faculty of Chemistry, Biological and Chemical Research Centre, University of Warsaw, Pasteur Street 1, 02-093 Warsaw, Poland

* Correspondence: mk.waclawska@uw.edu.pl (M.W.); wdzwolak@chem.uw.edu.pl (W.D.)

Abstract: Atomically precise noble metal nanoclusters protected by ligands are broadly discussed in the literature as a promising new class of materials with many interesting properties. Of those, the most prominent is the characteristic luminescence in the visible and near-infrared light. Within the plethora of conjugates of metal nanoclusters to various protective ligands, protein-enveloped systems present several unique features arising from an interplay of the nanocluster photophysics and the protein chemistry along its macromolecular dynamics. The specific properties of protein–metal nanocluster conjugates underlie various applications of these systems, especially in bioimaging. This review, in contrast to many already published, focuses on protein-protected gold nanoclusters (AuNCs) from the standpoint of the proteinaceous shell which plays a crucial role in the biocompatibility, solubility, and excellent in-solution stability of such nanohybrid complexes. Factors such as the protein's size, structural rigidity, amino acid composition, electric charge, and the electron donor properties of composite amino acids are discussed.

Keywords: nanomaterials; sub-nanometer materials; metal nanoclusters; protein-protected gold nanoclusters; bioinorganic materials

Academic Editor: Massimo La Deda

Received: 7 December 2024
Revised: 15 January 2025
Accepted: 17 January 2025
Published: 23 January 2025

Citation: Wacławska, M.; Dzwolak, W. Shedding Light on the Proteinaceous Envelope Protecting Luminescent Gold Nanoclusters: A Review. *Photochem* **2025**, *5*, 3. https://doi.org/10.3390/photochem5010003

1. Introduction

Noble metal nanoclusters are composed of a few to around a hundred atoms. In bulk metals, the electronic properties are generally described by continuous bands of energy levels. When the size of a metal nanoparticle becomes comparable to the Fermi wavelength of electrons, discrete energy levels due to the quantum effects start to dominate and the overall energy band structure becomes discrete. Nanoclusters, as well as quantum dots, nanowires, and nanocrystals, are examples of nanostructures exhibiting the quantum confinement effect: as the size of these structures decreases, the energy levels of electrons become quantized, leading to unique electronic and optical properties.

The critical size of the gold nanostructures for which the collective plasmon resonance is no longer important was provided by Qian et al. and was stated to be ~200–300 Au atoms, which is equivalent to the diameter of ~1.8–2.1 nm [1–3]. The cluster size is strongly intertwined with its properties, as the fraction of the surface atoms and the electronic structure are strongly dependent on the size of the nanocluster (and to a lesser degree, on its shape at a fixed number of atoms within the cluster—e.g., [4]). An excellent example is the possibility of tuning the emission wavelength of nanoclusters by changing their size: Au_{31}, Au_{25}, Au_{13}, Au_8, and Au_5 exhibit near IR, red, green, blue, and UV emission, respectively [5,6]. Arguably, among those nanocluster forms, the most researched has been the thiolate-stabilized Au_{25} ($Au_{25}(SR)_{18}$) known as "captain of the great nanocluster

ship" [7]. Over the recent years, this has yielded a plethora of detailed data on its fascinating photophysical and physicochemical characteristics (e.g., [8]). In particular, the seminal work on resolving the atomic structure of the thiol-capped Au_{25} and correlating it with time-dependent density functional theory (TD DFT) calculations provided key insights into the origins of AuNC optical properties [9]. The surface ligands of metal nanoclusters are critical in determining their shape, size, and interfacial characteristics, resulting in different optical properties. This optical tunability, combined with good photostability and the possibility of introducing a variety of surface modifications, makes these fluorescent structures an exciting class of nanomaterials with possible use in biolabeling and imaging [2,10,11], bioassays [12,13], electronic devices, sensors [14,15], and environmental analysis [16,17].

No fixed mechanism of luminescence emission is currently accepted. Many groups suggest that there is a mixed contribution of quantum confinement of the metal core and ligand-to-metal charge transfer, especially via Au-S bonding [18]. Xie et al. postulated that, while the structure of the Au core is the determinant of the energy associated with the observed luminescence, interactions between the Au surface and the capping agents are the key factor for its quantum yield. On the other hand, this seems not to be in agreement with the work of Liu et al., as they reported that different surface coverage of AuNC by glutathione results in the emission of different colors of light, independent of the core size [19].

It is also important to note that the usage of gold instead of other metals is not incidental. Gold is particularly attractive due to its superior resistance to oxidation, as opposed to silver in fluorescent silver nanoclusters [20]. Compared to other fluorescent nanomaterials, such as quantum dots, AuNCs do not contain toxic heavy metals. Moreover, gold exhibits excellent antibacterial capability [21].

2. Ligands Protecting Gold Nanoclusters

In solutions, AuNCs are usually protected from aggregation into larger nanostructures by ligands. These can include dendrimers [22–24], polymers [25–28], thiolates [29], ionic liquids [30,31], peptides [32], proteins [33], oligonucleotides [34], and DNA [35–37]. The variety of templates provides a wide range of possibilities of tailoring the final product to one's needs. The templates provide a variety of configurations and spaces, and can be used to synthetize metal nanoclusters of well-controlled morphology (in terms of core-size and shape). The scaffolds can also play an important role in the photophysical properties of the hybrid nanocomplexes. Last, but not least, some templates (e.g., peptides, proteins, and DNA) provide the nanoclusters with high biocompatibility, rendering them non-toxic and thus allowing their use in biological and medical sciences as fluorescent probes and sensors. The essential role of surface chemistry in establishing a stable protein corona is well recognized also in the case of larger non-luminescent metallic nanoparticles (AuNPs—[38]).

A short compendium of examples of AuNC–ligand complexes obtained to this date and some of their properties can be found in Table 1. Protein-protected AuNCs will be discussed in detail in the dedicated section.

Table 1. Examples of ligands used in the synthesis of ligand-protected gold nanoclusters. PAMAM stands for poly(amidoamine) dendrimers and the number refers to the generation of the used dendrimer.

Ligand	NC Size [*Estimated Number of Au Atoms]	Fluorescence Excitation and Emission Wavelengths [nm]	Ref.
PAMAM dendrimer, G9	4 nm	–	[22]
PAMAM dendrimer, G4-OH	[*Au_4]	382/445	[23]
poly(N-vinyl-2-pyrrolidone)	1.3 nm	–	[25]

Table 1. *Cont.*

Ligand	NC Size [*Estimated Number of Au Atoms]	Fluorescence Excitation and Emission Wavelengths [nm]	Ref.
poly(2-ethyl-2-oxazoline)	6.4 ± 0.2 nm	290/645	[27]
poly(1,2-butadiene)	[*Au_8], 1.4 nm	370/465	[38]
low density of glutathione	1.7 ± 0.2 nm	412/638	[28]
high density of glutathione	1.6 ± 0.2 nm	412/638	[28]
C5 DNA	–	370/455	[33]
SS DNA	2 nm	467/725	[34]
poly-C DNA	~2 nm	245/440	[35]
histidinehydroxamic acid	–	365/440	[39]
nicotinamide	~1 nm	335/380	[40]
lipoic acid	–	400/740	[41]
(3-mercaptopropyl)sulfonate 1-decyl-3-methylimidazolium	[*Au_{25}]	–	[29]
captopril	2.3 nm	362/414	[42]
penicillamine	<2 nm	400/610	[43]
4,6-diamino-2-mercaptopyrimidine	~6 nm	360/635	[44]

3. Protein-Protected Gold Nanoclusters

Biologically important proteins and peptides, as well as short custom-designed peptide sequences, are efficient scaffolds for the nucleation and growth of AuNCs. The usage of proteins in the template-assisted synthesis of metal nanoclusters introduced a number of advantages such as facile preparation, mild synthesis conditions, controllable and uniform size of obtained clusters, excellent water-solubility, and biocompatibility [31,32,45,46].

The generally applicable procedure of synthesis was first described by Xie et al. and was based on the biomineralization of a protein, BSA—bovine serum albumin [32] and can be summarized as pictured in Figure 1. This pioneering protocol calls for the addition of aqueous $HAuCl_4$ to the protein solution under vigorous stirring. Then, NaOH solution is introduced and the mixture undergoes incubation at a slightly elevated temperature (37 °C) for at least 12 h. The formation of protein-templated AuNCs is indicated by a change in the color of the solution from light yellow to deep reddish brown. The reaction time can be reduced by introducing microwave-assisted methods which provide uniform heating [47–50]. Some groups have modified this procedure by using auxiliary reducing agents, such as ascorbic acid [51]. Importantly, this protocol provides a versatile and effective paradigm for a pathway to protein-protected nanoclusters of other metals (such as Ag or Cu) [52].

To this date, a broad range of proteins have been used as protective corona for in situ formed AuNCs, including BSA [3,32], lysozyme [53,54], and enzymes such as pepsin [55], trypsin [56], horseradish peroxidase [14], and DNase [57]. A short summary of proteins used as ligands for the synthesis of AuNCs and some of the properties of the resulting AuNC–protein complexes can be found in Table 2. It is worth noting that the liberation of the AuNCs from the protein scaffolds cause coalescence into bigger (and thus nonfluorescent) nanostructures [58]. Hence, the stability of AuNC–protein luminescence depends in particular on the stability of a proteinaceous envelope. Should the latter be compromised in the presence of, for example, protein-degrading enzymes, this, in principle, could become a basis for devising assays to detect protease activity [59,60]. While there has been some debate as to the nature of the mechanisms underlying the protease-induced quenching of

protein–AuNC luminescence, it appears that the release of AuNCs and the subsequent coalescence into non-luminescent plasmonic nanoparticles (rather than, for example, the impact of environmental oxygen) is the actual culprit [61].

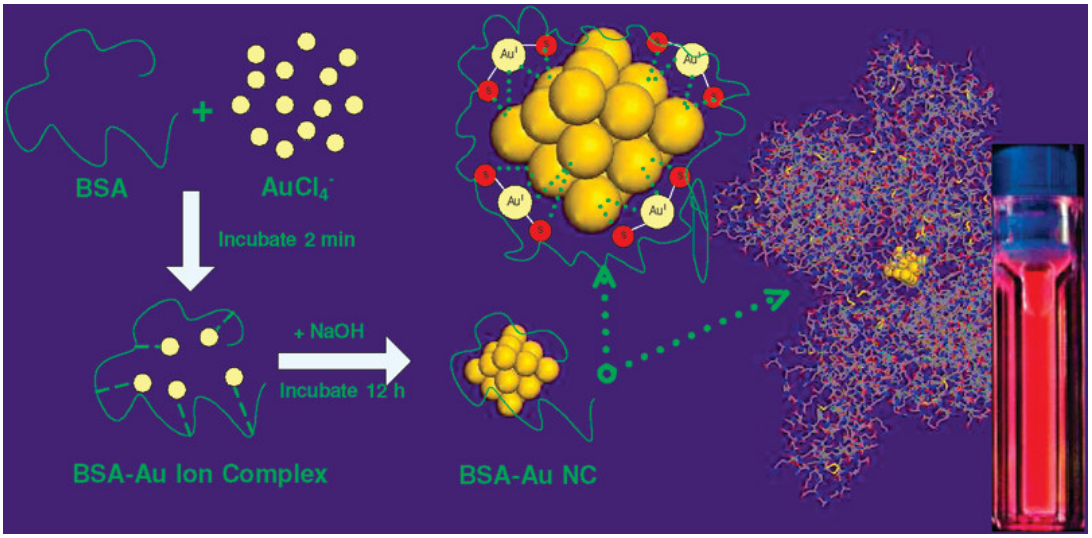

Figure 1. Schematic diagram of AuNCs' formation in the presence of BSA. Reprinted with permission from Ref. [32]. Copyright 2009 American Chemical Society.

Table 2. Proteins used for the synthesis of gold nanoclusters.

Ligand	NC Size [*Estimated Number of Au Atoms]	Fluorescence Excitation/Emission Wavelengths [nm]	Ref.
horseradish peroxidase	2.7 ± 0.6 nm	365/650	[14]
bovine serum albumin	[*Au_{25}]	470/640	[32]
horse hearth myoglobin	[*Au_8]	495/450	[52]
bovine hearth cytochrome c	[*Au_8]	495/450	[52]
bovine plasma fibrinogen	–	–	[52]
bovine milk β-lactalbumin	[*Au_8], [*Au_{25}]	495/450 and 495/~650	[52]
bovine pancreas α-chymotrypsin	[*Au_8], [*Au_{25}]	495/450 and 495/~650	[52]
lysozyme	4 nm	370/650	[53]
lysozyme	3.84 ± 0.52 nm	470/650	[54]
pepsin	[*Au_{25}]	360/670	[55]
trypsin	2.7 ± 0.4 nm	520/690	[56]
DNAse I	[*Au_8], [*Au25]	395/460, 490/640	[57]
bovine serum albumin	[*Au_8], [*Au_{13}]	330/410, 330/510	[62]
human serum albumin	2 nm	474/609	[63]
insulin	3.5 ± 0.4 nm	400/670	[64]
trypsin	<3.0 nm	520/650	[65]
papain	1.2 ± 0.2 nm	470/660	[66]
transferrin	<2 nm	390/695	[67]
lactoferrin	<1 nm	445/650	[68]
hemoglobin	<10 nm	365/450	[69]
hemoglobin	3.7 nm	314/430	[70]
hemoglobin	[*Au_{25}]	494/654	[71]
soy protein	<2 nm	480/630	[72]
ovalbumin	3.8 nm	490/650	[73]

Table 2. *Cont.*

Ligand	NC Size [*Estimated Number of Au Atoms]	Fluorescence Excitation/Emission Wavelengths [nm]	Ref.
Apo-α-lactoalbumin	~2 nm	365/450 and 365/660	[74]
bromelain	–	350/430	[75]
BSA and bromelain	1.5 nm	495/633	[75]
avidin	5.6 ± 1.4 nm	374/449 and 374/651	[76]
herceptin	8.4 nm	488/645	[77]
gluten	2.78 nm	370/640	[78]
BSA and lysozyme	2.8 nm	500/640	[79]
L-tyrosine	1–3 nm	385/450	[80]
CD33 monoclonal antibody	AuNC size < 1 nm in spherical aggregates of size ~12 nm	510/656	[81]

As can be easily noted, the sizes of nanoclusters reported in the literature vary greatly. Interestingly, in some cases, the measurements from TEM images of AuNCs exceed the size that is considered crucial for their fluorescent properties (the maximum of 2 nm in diameter). The observed discrepancies can be attributed to differences in the synthesis conditions but also to the systems which were used to obtain measurements. It is a known fact that the focused electron beam of HR-TEM (High Resolution Transmission Electron Microscopy) can lead to changes in the size and shape of metal nanostructures as well as changes in their structure [82–85]. When dynamic light scattering (DLS) is used for the size estimation, one should take notice that the average hydrodynamic diameter according to DLS in solution is usually of a higher value than the average particle diameter as found by HR-TEM, which was measured under an ultrahigh vacuum, especially in the case of inorganic–organic nanocomposites like protein-protected nanoclusters. Mass spectrometry (MS) is yet another method used to estimate the size of protein-protected AuNCs. In this indirect method, the mass of a protein monomer is subtracted from the mass of the protein–AuNC conjugate. However, this approach is inherently inaccurate, as the conjugates are polydisperse (Au atoms are not confined to a single binding site within the protein molecule (they may be distributed across various cysteine and other residues in the protein)). Furthermore, one should take into account the possible fragmentation and partial degradation of the protein ligand occurring prior to the measurement.

4. Protein Size and Ligand to Gold Precursor Ratio

The protocol provided by Xie et al. works well for a wide variety of protein ligands encapsulating luminescent metal NCs. Volden et al. employed a similar protocol (protein is dissolved in PBS buffer instead of distilled H_2O with the mixed reactant samples kept at 37 °C for a week) to synthetize AuNC with eight proteins: bovine serum albumin (BSA), bovine milk α-lactalbumin type I (BLA), horse heart myoglobin (Mb), chicken egg white lysozyme (Lyz), bovine pancreas α-chymotrypsin (CTR), bovine plasma fibrinogen (Fib), bovine milk β-lactoglobulin (BLG), and bovine heart cytochrome c (Cyt) [52]. By using the same synthesis protocol for these eight proteins, the effects of protein size, overall protein charge (pI), conformational flexibility, and the occurrence of specific amino acid residues on the ability to reduce and stabilize gold nanostructures were probed. Among these proteins, only Fib produced non-luminescent clusters. Luminescence from BLG-NC was low, but detectable. While Fib is the heaviest of used proteins (340.0 kD), the molecular weight of BLG (18.0 kDa) is not very different from other proteins (CTR: 25.0 kDa, Lyz: 14.2 kDa). BSA, which produces BSA-AuNC with high quantum yield, weighs 67.0 kDa. Hence, it is hard to point to a general and clear relationship between the weight of the protein involved

and the quantum yield of luminescence of its conjugate to AuNCs. This is supported by the fact that it is possible to synthesize fluorescent AuNC using short peptides [31,86].

Another lead that was being followed in the context of nanocluster synthesis concerned the stoichiometry of protein–gold precursor mixing. When AuNCs were synthesized using His and Trp [81], a too low ratio of ligand to gold compound resulted in non-luminescent products. On the other hand, with the ligand excess, the fluorescence intensity increased to a maximum value and then decreased [87,88].

5. Structural Rigidity of the Protein

Both the effect of the spatial structure of the protein on synthesized AuNCs and the effect of synthesized AuNCs on the protein's structure are not fully explored yet; it is often the case that studies discussing the syntheses of fluorescent complexes lack a detailed spectroscopic characterization of the proteinaceous envelope's structure. It is expected that the encapsulation of Au nanoclusters inside the protein template affects the protein structure [89]. From the available data including our own work, we conclude that the strongly alkaline reaction environment used in most of the syntheses results in a partial loss of the protein's secondary structure. Examples include the experiments by Yarramala et al. [74], Rajamanikandan et al. [90], and Kluz et al. [91]. Although these works focus on different proteins (apo-α-lactalbumin, ovalbumin, and bovine serum albumin, respectively), in each case, significant differences in the circular dichroism spectra (CD) between the native protein and its AuNC-bound form were observed. As shown in Figure 2, Kluz et al. compared three different protein forms: unmodified, native BSA, BSA subjected to a prolonged incubation in an alkaline environment without a gold precursor (BSA-Alk), and BSA-AuNC. According to the spectroscopic data, the addition of NaOH required in Xie's protocol results in a roughly 20% decrease in the ellipticity, implying a corresponding amount of disruption of the native α-helical structure of BSA. In BSA-AuNC, an even more pronounced decrease in ellipticity was observed (~50%). A strongly alkaline environment results in the unfolding of the native α-helical structure, the disappearance of tertiary contacts, and even, in this case, the hydrolysis of disulfide bridges, as shown by Raman spectroscopy [92].

The hydrolysis of disulfide bridges was also observed during the synthesis of lysozyme–AuNC and it was interpreted as the main reason for the significant decrease in helicity [93]. Interestingly, reports on bovine insulin–AuNCs show intact S-S bridges [64,94]. Nonetheless, CD spectroscopy clearly shows that the BSA bound to AuNC in the BSA-AuNC complex is significantly disordered and retains only a fraction of the native conformation. In fact, the partial denaturation of BSA under the alkaline conditions of BSA-AuNC synthesis is not only an immediate response of the protein structure to the extremely high pH, but it also becomes more pronounced on the time-scales of the synthesis, just as the complex chemistry leading to the formation of AuNCs is progressing. Figure 3 shows a time evolution of the secondary-structure-sensitive far-UV CD spectra of BSA in the presence of NaOH and $HAuCl_4$ (at the ratio and concentrations as required in the Xie's protocol) along with the accompanying changes in the near-UV region corresponding to the tertiary contacts of aromatic residues. The plotted time-dependent changes in ellipticity at 222 and 270 nm are juxtaposed to those of BSA subjected to an analogous alkaline treatment in the absence of $HAuCl_4$, allowing one to appreciate how detrimental to the native fold are the basic conditions rather than the formation of AuNCs per se. It is worth mentioning that, according to a previously reported CD-based investigation, an addition of pre-formed larger non-fluorescent AuNPs to native BSA also results in a modest decrease in the protein's helical content [95]. However, the patterns of protein–Au interactions in both these cases (i.e., the in situ formed BSA-AuNC conjugate and the electrostatic BSA-AuNP

complex) are expected to be distinct; therefore, the mechanisms underlying the partial unfolding are also likely to be different.

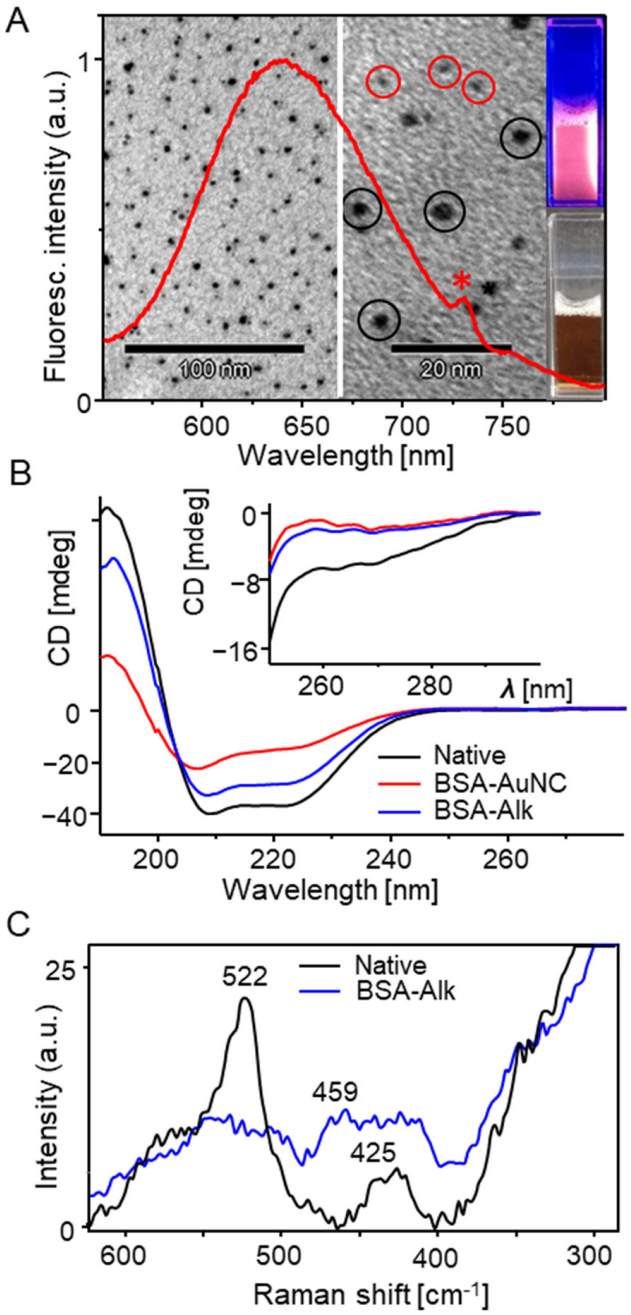

Figure 2. (**A**) Luminescence emission spectrum of BSA-AuNC (λ_{exc} = 365 nm) overlaid on unstained TEM images of BSA-AuNC; AuNCs of a diameter below 1 nm are marked with red circles whereas larger non-fluorescent AuNPs are in black circles; sharp peak marked with an asterisk corresponds to scattered $2\lambda_{exc}$ light. Photographs of BSA-AuNC liquid sample illuminated with 365 nm UV light (top), and in daylight (bottom) are on the right. (**B**) Far-UV CD spectra of native BSA, BSA-Alk, and BSA-AuNC collected at the same protein concentration and pH 7; inset shows the corresponding near-UV CD spectra. (**C**) Raman spectra of native BSA and BSA-Alk (laser line 780 nm). Reprinted from Ref. [91].

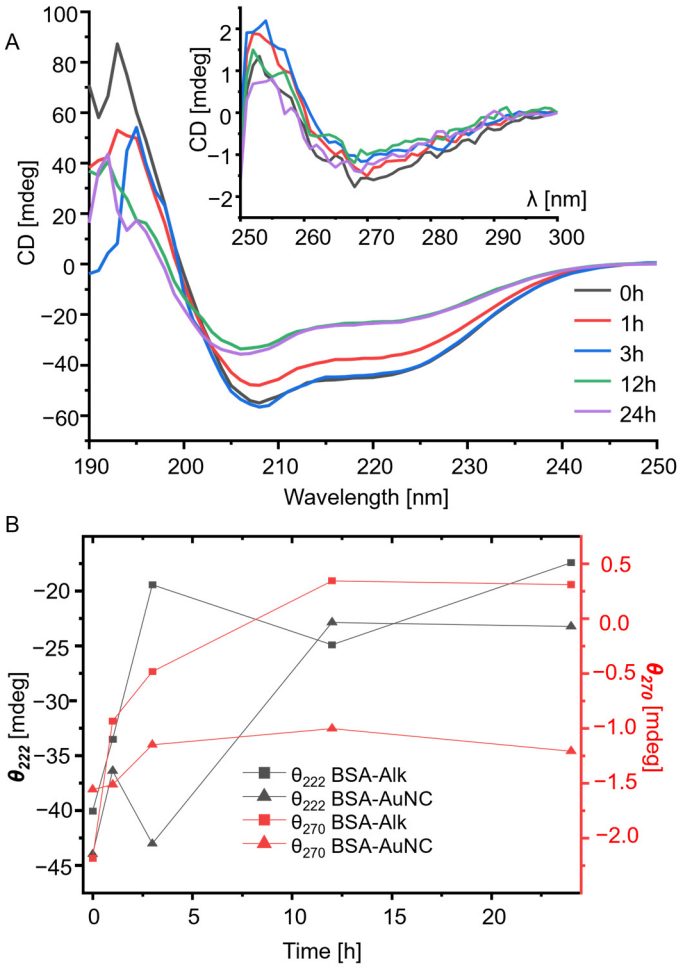

Figure 3. (**A**) Time-lapse far-UV CD spectra of BSA under the conditions of formation of BSA-AuNC conjugate (a protocol similar to Xie's approach: 25 mg/mL BSA in 5 mM $HAuCl_4$ and 0.1 M NaOH, 37 °C, 600 rpm agitation, other data collection details as in the work Kluz et al. [85]). In the inset, the corresponding near-UV CD spectra are shown. (**B**) Plotted time-dependent ellipticity values at 222 and 270 nm for the samples in which the actual BSA-AuNC synthesis takes place compared with control data on samples lacking $HAuCl_4$ (BSA-Alk).

As UV absorption by residual Au compounds and already formed AuNCs, as well as the scattering of short-wavelength UV light, can compromise quality and hamper the interpretation of UV-range CD spectra, complimentary approaches have been used to analyze the state of protein ligands binding AuNCs. One such approach is Fourier-transform infrared spectroscopy (FT-IR) in the secondary structure-sensitive amide I frequency range. Examples of spectra of insulin-AuNC can be found in Figure 4. Changes in amide I peak position, intensity, and spectral contour shape can indicate alterations in protein conformation induced by factors such as pH, temperature, or ligand binding. Cun et al. collected FT-IR spectra of freeze-dried hemoglobin and hemoglobin–AuNC (Hb-AuNC) [71]. In comparison to the native sample, the spectrum of Hb-AuNC showed broader peaks and a number of features were merged together. The amide I band was shifted towards shorter wavelengths and lost some of its initial intensity while the neighboring amide II band was shifted towards longer wavelengths with its intensity relatively increased. Similar changes in the position of the amide II band were observed by Guével et al. [67] and Ghosh et al. [65]. Moreover, the spectrum of Hb-AuNC exhibited an additional band at 1430 cm^{-1}. This was also reported previously and can be attributed to the CH_2 bending of protein's hydrophobic residues which, due to the protein unfolding, are exposed after the formation of protein–gold nanoclusters [88]. The corresponding second derivative spectra

have shown that the main component of native hemoglobin is the α-helix whereas, upon the incorporation of AuNCs, the α-helix content is significantly decreased and the content of random coils, β-sheet, and intermolecular aggregates increased [71]. This points to the fact that—upon the formation of nanoclusters—the secondary and tertiary structures of proteins change. Therefore, it is interesting to probe how a more rigidified structure of protein shell affects the properties of the protein–AuNC conjugate.

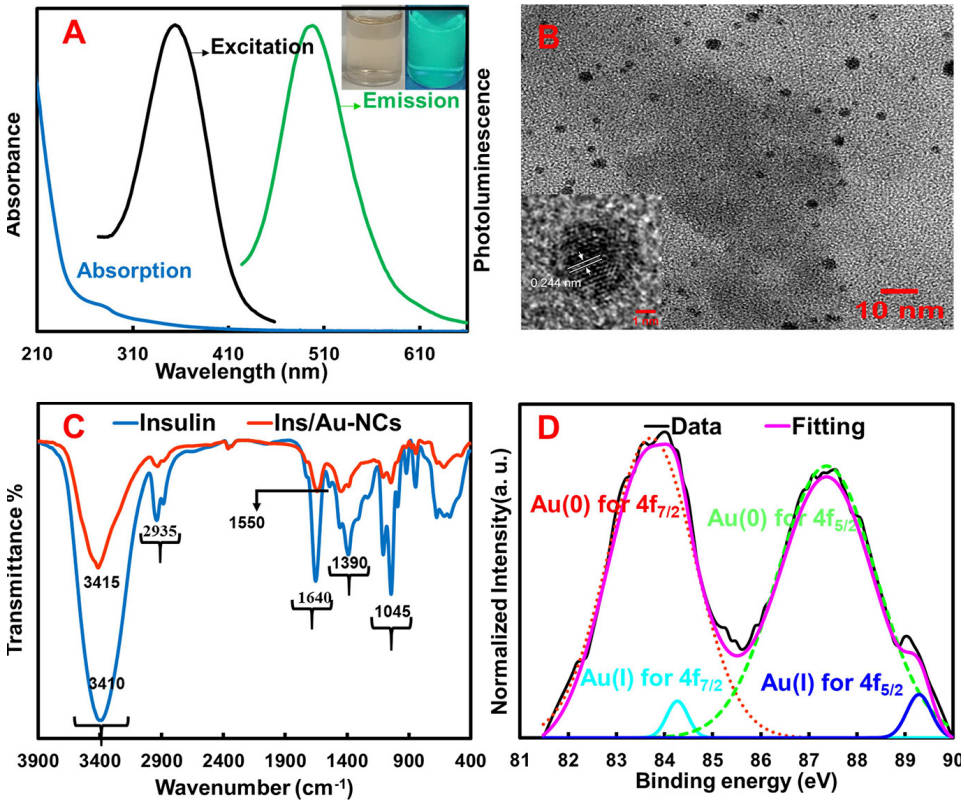

Figure 4. (**A**) UV−Vis absorption spectrum and fluorescence excitation and emission spectra of Ins-AuNCs. The inset shows the photographs of Ins-AuNCs solution in daylight and 365 nm UV light. (**B**) TEM image and HR-TEM image of single AuNCs (inset). (**C**) FTIR spectra of Ins-AuNCs and insulin. (**D**) XPS results of Ins-AuNCs. Reprinted with permission from Ref. [93]. Copyright 2023 American Chemical Society.

BSA is known to undergo conformational changes in response to variations in pH levels. The protein has five distinct structural monomeric forms: E (extended, under pH 2.7), F (fast migration), N (normal, between pH 4.3 and 8), B (basic, pH above 8), and A (aged, above pH 10) [96]. Yu et al. inquired how the pH of reaction mixture affects the ability of BSA to form BSA-AuNC. By varying the pH, both Au_{25}NC (in pH ~11) and Au_{13}NC (in pH 7.4) were obtained at a constant Au–BSA ratio of 24:1. The α-helix content of the conjugates was probed using CD spectroscopy and for BSA-Au_{13}NC and BSA-Au_{25}NC, the values were subsequently 36.8% and 18.2%, respectively. Interestingly, at pH 7.4, a complex containing a maximum of 13 gold atoms was formed, regardless of the Au–BSA ratio used (even when the ratio of 47:1 was tested), highlighting the role of BSA conformation in aqueous solution determining the size of AuNCs in BSA-AuNC complexes [97]. Another brilliant example of how the conformation of protein controls the size of nanoclusters was presented using apo-α-lactalbumin: a milk protein possessing a single binding site for Ca^{2+}. Apo-α-lactalbumin can also bind La^{3+} with a high affinity. It was found that when the binding site is occupied with a metal ion, the protein envelope restricted the growth of AuNCs, demonstrating the potential of controlling the size of resulting clusters. In the

absence of La^{3+} ions in the solution, a core size of Au_{10} was observed. When the La^{3+} ions were added, nanoclusters with a core size of 6 to 10 Au atoms were formed, depending on the concentration of La^{3+} added. Their spectra are shown in Figure 5. The synthesis of AuNCs protected with apo-α-lactalbumin in the presence of Ca^{2+} resulted in Au_8NCs and with Gd^{3+} a mixture of Au_nNC, where n = 7, 8, 9 [79].

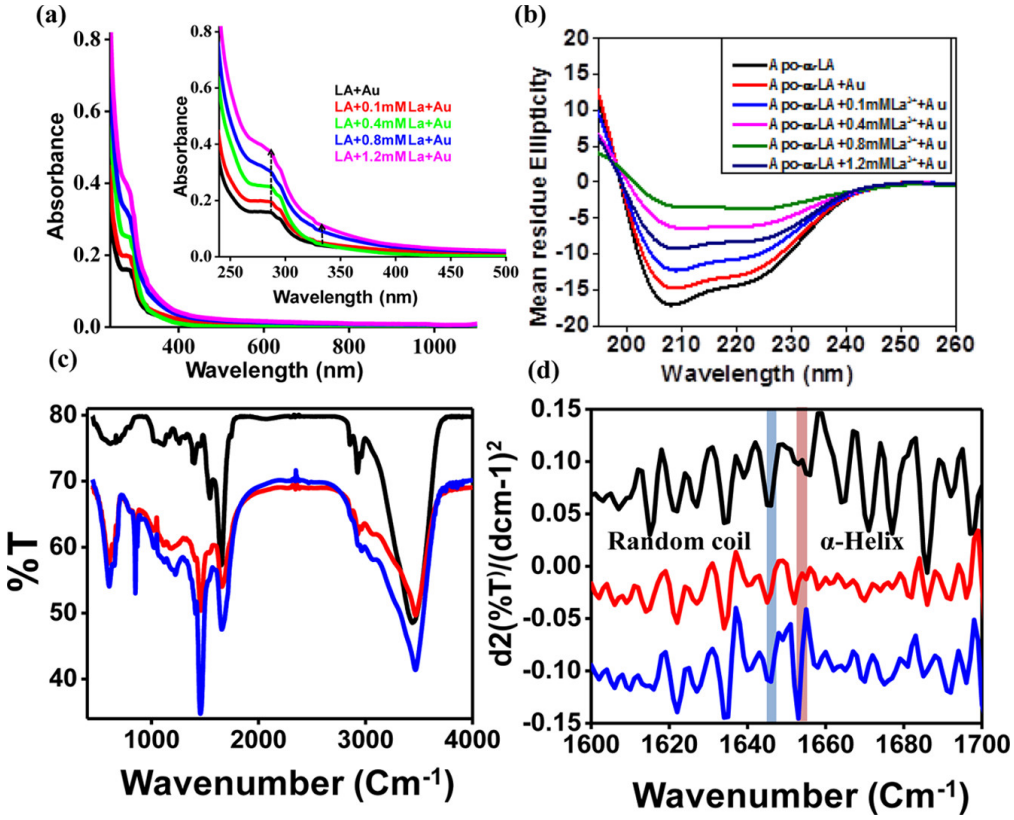

Figure 5. Spectra of concentration-dependent La^{3+}-incorporated α-LA: (**a**) absorption spectra, (**b**) CD, (**c**) FT-IR apo-α-LA (black), α-LA-AuNCs (red), α-LA-1.2 mM La^{3+}-AuNCs (blue), and (**d**) double derivative of FT-IR, color-coded with blue at 1654 cm^{-1} for random coil and pink at 1648 cm^{-1} for α-helix. Reprinted with permission from Ref. [74]. Copyright 2017 American Chemical Society.

Fatty acids are known to stabilize albumin structure, causing it to be more resilient to environmental changes such as varying temperature or different pH levels [98–100]. This inspired an interesting question on how the content of fatty acids interplays with BSA determining the characteristics of BSA-AuNCs. Data on this subject were provided by Andrýsková et al. [100] who used three different types of BSA: commercially available 98% BSA, 96% BSA, and 98% fatty acid-free BSA (denoted as df98BSA). These were used as substrates in a microwave-assisted synthesis of BSA-protected AuNCs. The resulting products were then evaluated for their alpha helix content. The increase in structural disorder was more pronounced in df98BSA, as compared to the samples containing fatty acids according to the data provided by calculations based on FT-IR and CD spectra. According to fluorescence spectroscopy measurements, the presence of fatty acids in albumin leads to an increase in the fluorescence intensity. When df98BSA was modified with palmitic acid, both prior and after the synthesis of AuNCs, the quantum yields had similar values (around 7%), higher than the quantum yield of unmodified, fatty acid-free BSA-AuNC (around 5.7%). The researchers arrived at the conclusion that the fluorescence increase stems from the rigidification of albumin structure.

6. Amino Acid Composition

The amino acid composition can vary significantly from protein to protein; thus, it is only natural to expect that the synthesis of protein-protected nanoclusters might yield different products depending on the protein in question. While approaching the complex problem of the role of individual amino acid residues in the formation and stabilization of protein–AuNC conjugates, one has to take into account the empirical fact that distinct (in terms of amino acid compositions, but also molecular weight and pI—see Figure 6) proteins can give rise to conjugates with very similar (BSA and HEWL) or very different (BSA and Cyt C) photophysical properties. Hence, the end photophysical properties of these systems are outcomes of a complex interplay of many factors as opposed to being determined by a single dominating protein feature, such as high content or aromatic residues.

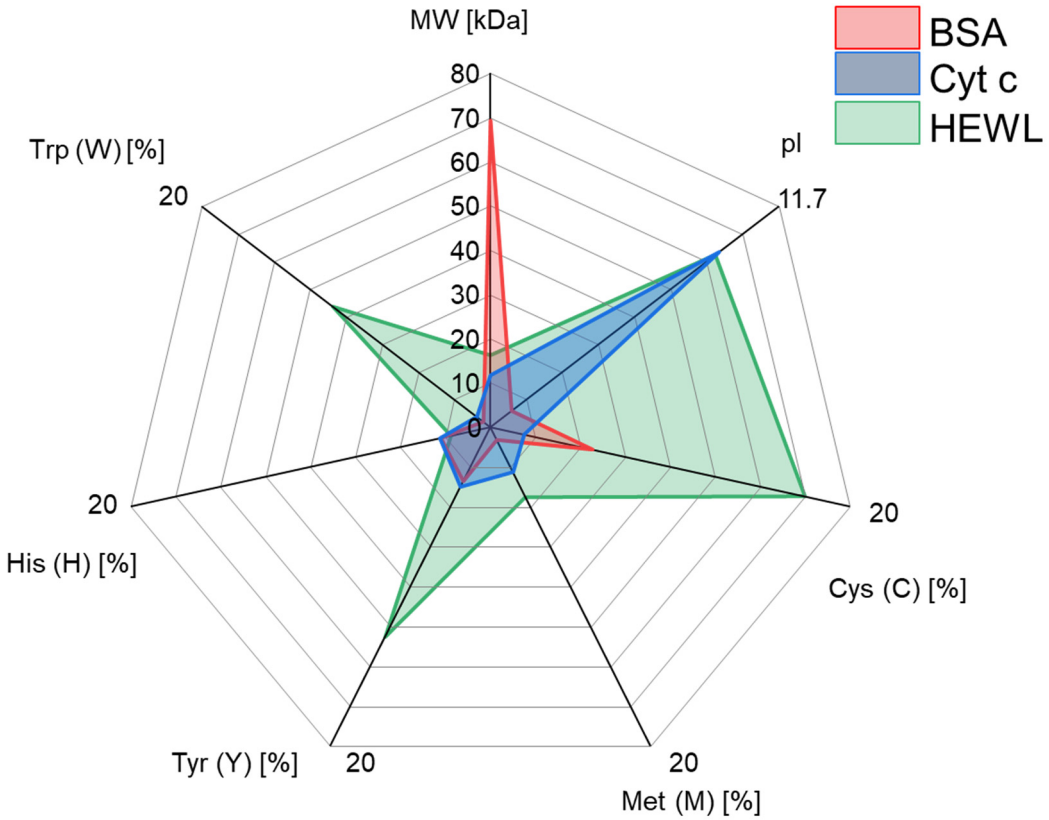

Figure 6. Radar plot of several local (relative amino acid content (per cent) of Trp, His, Tyr, Met, and Cys residues) and global (isoelectric point, molecular weight) properties of three proteins: BSA, HEWL, and Cyt c, giving pairwise similar (BSA and HEWL) and quite distinct (Cyt c and BSA) photophysical properties of AuNC conjugates.

BSA-AuNCs demonstrate a strong emission upon excitation with UV light with peaks around 450 nm and 650 nm, indicating the presence of both small and large gold nanoclusters. In contrast, Cyt c-AuNCs emit weaker fluorescence in blue and purple light regions. This difference can be attributed to a low concentration of small gold nanoclusters in the product or to aromatic amino acid side groups. Notably, Cyt c-AuNCs also exhibit a blue shift and a weakening of the absorption band at approximately 410 nm, implying that the formation of gold nanostructures affects the environment surrounding the heme group in cytochrome c.

Natural amino acids possess the ability to bind to Au atoms owing to their chelating and functional groups, such as amine, carboxyl, and thiol. According to Tan et al., the peptide-driven formation of AuNC requires the presence of amino acids exhibiting two

functions: a capacity to reduce the gold ions to gold atoms and a strong ability to bind to the surface of forming gold [101].

Li et al. conducted a theoretical study in which the reactive abilities of 20 naturally occurring amino acids were approximated by their HOMO/LUMO energy gap analysis through DFT calculations [102]. According to this study, tryptophan, histidine, and tyrosine are the strongest reducing agents while methionine and cysteine—both containing S atoms—allow the strongest binding of Au by forming Au-S bonds. Further theoretical studies provided insight into the binding affinity of amino acids to Au^+. Among all the amino acids naturally occurring as building blocks of proteins, cysteine with its deprotonated side chain (denoted as <<Cys(-H^+)>>) had the highest value of the Gibbs free energy associated with Au^+ binding with amino acids [103]. This is in agreement with the DFT study by Srivastava, in which the intermolecular interactions between gold nanoclusters Au_n (n = 8, 10, 12) with cysteine in its neutral and ionic forms were investigated. According to the results of this study, cysteine can form stable complexes with gold. The cationic form of cysteine interacts with gold most strongly and the bonding energy is inversely correlated to the Au-S bond length [104]. According to another TD-DFT study, the impact of ligands on luminescence will be particularly pronounced in the case of very tiny (Au_2 and Au_4) clusters [105].

The interactions between Au and S have also been discussed in the context of fluorescence emission mechanisms. It was proposed that the fluorescence emission of Au_{25}-NC originates from a Au_{13} core decorated with 6 staple surface motifs: -S-Au(I)-S-Au(I)-S-, suggesting that 18 cysteine residues are required for the fluorescence [106–108]. However, fluorescent insulin–AuNC [64,95], pepsin–AuNC [55], trypsin–AuNC [56], and myoglobin–AuNC [52] were synthesized and these proteins contain only 6, 6, 7, and 0 cysteine residues, respectively. This points to two possible scenarios: either amino acids other than cysteine start to contribute to the stabilization of the emerging nanoclusters or multiple protein molecules are involved in the synthesis process.

Liu et al. in 2011 proposed that the synthesis of insulin–AuNC differs from the mechanism of BSA-AuNC, as no Au attached to the insulin was detected in mass spectrometry after the synthesis of a fluorescent insulin–Au nanocomplex [64]. This differs from BSA, for which clear BSA-AuNC peaks are observed [109]. The group points to the fact that insulin has only six cysteine residues, all of which are involved in S-S linkages between chains A and B; hence, interactions between gold and other residues such as tyrosine, lysine, aspartic acid, arginine, and tryptophan are more likely. Such polar interactions would be weaker than the covalent Au-S linkage and thus possibly not observable in mass spectrometry. This is also supported by Raman spectroscopy. Namely, before and after the growth and encapsulation of AuNCs, the S-S stretches arising from intact S-S crosslinking are visible in the Raman spectra, as observed by both Liu et al. and Shamsipur et al. [94,110].

Xu et al. have argued that while thiol groups form chemical bonds with Au surfaces, amine groups can form coordination bonds and can also be involved in the stabilization of Au nanoclusters; the pI of proteins before and after the nanocluster encapsulation in the case of trypsin and lysozyme were significantly reduced (from 7.0 and 10.5 to 5.0 and 5.5, respectively), while the pI of BSA containing 35 cysteine residues remained unchanged after the encapsulation [89].

In 2023, Peng et al. first proposed a machine-learning-based model designed to search for the factors affecting the binding affinity of small Au clusters (3 atoms) and amino acids in the gas phase and when solvated by H_2O considering single-site adsorption, not an actual solution environment [111]. According to this work, different environments result in different interactions between gold and amino acids: in the gas phase, the most stable complex of Cys-Au_3 is the one where gold is bonded with nitrogen atoms of amino groups, while in solution binding, through a sulfur atom is more favorable.

The earlier work by Abdalmoneam also probed amino acids in the gas phase and in solution, but was limited to alanine and tryptophan with Au_8 and Au_{25} [112]. Electrostatic potential (ESP) isosurfaces of the Au_8–Trp complex are depicted in Figure 7. The results showed that the amine N atom was energetically preferred for canonical forms of Ala and Trp but for their zwitterions, the carboxylic O was a favored bonding site. It has been also shown experimentally that in pepsin, the acidic amino acids rich in carboxyl groups (such as aspartic acid) can reduce $AuCl_4^-$ ions in acidic conditions [55]. However, such a reductive process is expected to be much slower than an analogous one involving tyrosine residues of pepsin in alkaline pH.

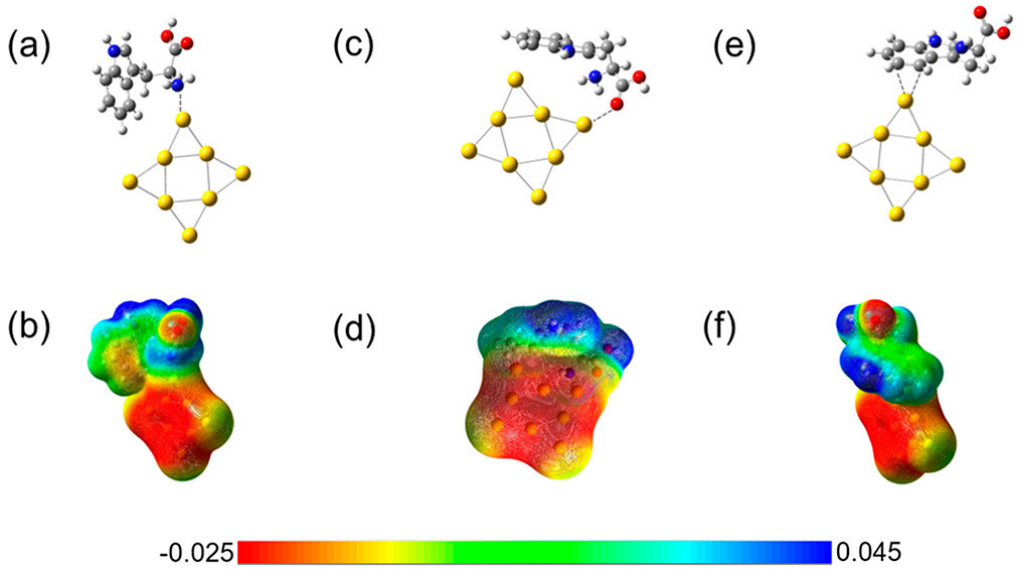

Figure 7. Gas-phase equilibrium configurations and ESP isosurfaces of the Au_8–Trp complex: (**a**,**b**) amine site, (**c**,**d**) carboxylic site, and (**e**,**f**) indole site. The colors in the figure range from red (most negative) to blue (most positive), with green representing a neutral charge. Reprinted with permission from Ref. [112]. Copyright 2017 American Chemical Society.

Advancing the understanding of how nanoclusters interact with amino acids will hopefully facilitate the design of target-specific bioimaging probes. In fact, such attempts have already been made; for example, Wang et al. designed a peptide with two functional domains. One of the domains (CCY) was responsible for the reduction of Au ions to Au nanoclusters and the second (derived from HIV-1 TAT protein) possessed targeting ability towards a cell nucleus [113]. Later, the same sequence of domain 1 was used by Song et al. [114] and Yuan et al. [115]. Yuan et al. coupled the CCY sequence (core sequence, denoted as *c*) to a short fibril-forming peptide KFFAK (assistant sequence, denoted as *a*) and used different motif combinations for the synthesis of AuNC. Interestingly, among these combinations, only *ca* and *aca* produced visible fluorescent complexes with AuNC when the concentration of the gold precursor and ratio of peptide to gold ions were kept the same, indicating the significance of motif sequences. The group speculates that the formation of fluorescent peptide–AuNC is governed by either steric hindrance or collision rate in solution; the heavier the sequence, the slower the peptide diffuses in solution and provides less opportunity for collision with gold ions. The formation of nanofibrils was observed, but the AuNCs were not well aligned with the fibrils according to TEM and AFM.

Another example of a designed sequence targeted towards the synthesis of AuNCs was provided by Lopez-Martinez et al. This group used a series of designed consensus tetratricopeptide repeat (CTPR) proteins to explore the effect of the coordinating protein on the properties of originally non-emissive “naked” AuNCs. CTPR proteins consist

of repeating 34-amino acid alpha-helical motifs. Two such proteins were constructed: WT(C_{4his})$_4$WT and WT(C_{4cys})$_4$WT, where WT stands for the wild-type CTPR motif and C_{4cys} or C_{4his} represents mutated CTPR motifs, where the metal coordinating residues were introduced in the positions 2, 6, 9, and 13 of the CTPR motif based on the Protein Data Bank crystal structure of entry 2HYZ. As a control, the CTPR-16glu protein with glutamic acids in the coordinating positions was used. As expected, the luminescent products were synthesized only with WT(C_{4his})$_4$WT and WT(C_{4cys})$_4$WT. Interestingly, as shown in Table 3, the chemical identity of the amino acid used for the metal coordination encoded a different emission wavelength of the resulting protein–AuNC complex upon excitation with the same wavelength at 390 nm, despite being of similar size [116].

Table 3. Characteristics of CTPR-AuNC obtained by Lopez-Martinez et al. [116].

Protein	Size [nm]	Excitation/Emission Wavelengths [nm]
WT(C_{4his})$_4$WT	1.7 ± 0.5	390/515
WT(C_{4cys})$_4$WT	1.7 ± 0.3	390/675

The group argues that, according to the mass spectrometry data, the blue-emissive histidine-coordinated AuNCs are only slightly larger than the red-light-emitting cysteine-coordinated AuNCs, so the prominent change in their luminescent properties is rather related to the capping ligands. When AuNCs were conjugated to cysteine and histidine using the same protocol and stoichiometry as for the CTPR protein conjugates, the resulting products were non-luminescent, which seems to support the idea that the protein's surface is of critical importance in the context of the optical properties of the bound AuNCs [116].

7. Charge and Electron Density of the Ligand

The polar amino and carboxylic groups have been reported as the favored anchoring sites for AuNCs both experimentally and theoretically, as widely discussed in the previous section. A number of studies have shown that the strength of interactions between amino acids and gold is related to the polarity of amino acids and its size [105,111,112,117,118].

Most protocols for the synthesis of protein-protected AuNCs call for a highly basic reaction environment. When the solution pH is above the pI value, the protein's net charge becomes negative. The exact value of the charge will depend on the protein's specific amino acid composition. The surface ligands impact not only the net charge but also the polarity of protected AuNCs. To our best knowledge, the extent to which the fluorescence from protein-protected nanoclusters is governed by the charges within the protein scaffold has not been thoroughly investigated to this date. Moreover, as discussed earlier in the text, the mechanism of fluorescence emission of AuNCs remains unclear.

Prieto and co-workers synthesized so-called naked gold nanoclusters: non-luminescent water-dispersible AuNCs without organic ligands. Those AuNCs require subsequent coating with ligands such as cysteines or adenosine monophosphate in order to become luminescent and emit in different spectral regions [119]. This clearly shows that conjugating the AuNCs to a ligand is a necessary step to obtain luminescent properties.

Wu and Jin proposed three routes of increasing the fluorescence of AuNCs: (i) increasing the ligands' capability to donate charges, (ii) increasing the electropositivity or oxidation state of the metal core, and (iii) employing ligands possessing more electron-rich atoms and groups [107]. Those ideas were widely discussed, especially in the context of thiol-protected AuNCs. However, Xu et al. replaced glutathione with short, custom tripeptides, Lys-Cys-Gly (KGG), Glu-Cys-Lys (ECK), and Glu-Ala-Gly (EAG), and observed that the fluorescence intensity of AuNCs protected with those tripeptides parallels their capacity to donate electrons to the metal core through Au-S bonding [28]. Both Xu et al. and Zhu et al.

agree that the use of ligands which contain more electron-rich atoms or groups (such as N or -NH_2) is an efficient strategy to enhance the luminescence of AuNC by strengthening the charge transfer between the ligands and Au core [28,120]. Similar experiments with amino acids were conducted by Wang et al. [121]. This group replaced BSA by conjugating the AuNC via a thiolatepoly(ethyleneglycol) linker with amino acids. The amino acids chosen for this task were divided into two groups: ones that contained neutral groups and ones containing electron-rich groups. Although the fluorescence intensity of such prepared hybrid nanocomplexes was weaker than that of BSA-protected ones, no significant difference was observed between ligands bearing neutral and electron-rich groups.

8. Applications of Protein-Protected Gold Nanoclusters

The use of AuNCs protected by biomolecules in medicine and bioimaging is widely discussed in the literature. Research points to several factors that speak in favor of using AuNCs over conventional fluorophores in certain fields. The main ones being their unique optical properties in the second near-infrared window (NIR-II corresponding to the 1000–3000 nm wavelength range) which, due to reduced photon absorption and scattering, allow for high-resolution imaging of internal organs, blood vessels, and tumors [122–125]. It should be stressed that there are some highly developed strategies to link preformed NIR-II emitting AuNCs to biocompatibility-providing proteins. Some of them purposely avoid direct metal–protein bonding interactions (e.g., by being mediated through host–guest interactions between β-cyclodextrin immobilized on the AuNC surface and adamantane bonded to BSA molecules, as is the case in the study by Song et al. [126]). As a consequence, the significant spatial separation between the nanocluster and the proteinaceous envelope may limit the scale of perturbation of the native structure. It has been demonstrated that the NIR-II luminescence of thiol-decorated Au25 nanoclusters may be tuned by functionalization with proteins [127]. It should be also stressed that there are some highly developed strategies to link preformed NIR-II emitting AuNCs to biocompatibility-providing proteins. Some of them purposely avoid direct metal–protein bonding interactions (e.g., by being mediated through host–guest interactions between β-cyclodextrin immobilized on the AuNC surface and adamantane bonded to BSA molecules, as is the case in the study by Song et al. [126]). As a consequence, the significant spatial separation between the nanocluster and the proteinaceous envelope may limit the scale of perturbation of the native structure. It has been demonstrated that the NIR-II luminescence of thiol-decorated Au_{25} nanoclusters may be tuned by functionalization with proteins [127]. It should be also stressed that the pharmacokinetics of AuNCs is also very favorable: the AuNC–conjugates show short distribution half-time, minimal accumulation in the reticuloendothelial system, and exhibit efficient renal clearance [128,129]. Au_{25}NCs were distributed within 1 min after injection, the transport from liver to bladder occurred after 10 min, and no significant signal in the bladder was observed after 24 h [130]. Another study provides neuroelectrophysiological monitoring data, according to which no permanent damage or toxic responses were revealed, irrespective of the Au_{25}NCs dosage [131]. Recently, Guo et al. have conducted a comprehensive study on the impact of various small ligands on the NIR-II bioimaging properties of small AuNCs containing 8 or 7 Au atoms [132].

Luminescent AuNCs attract a lot of attention because of their good photostability and high Stokes shifts. Therefore, AuNCs were explored as optical probes for bioimaging and in fluorescence sensing and biological detection [133]. Zeng et al. developed an application of lysozyme-protected gold nanoclusters (Lys-AuNCs) as dual-emission probes for the ratiometric sensing of cyanide by fluorescence resonance energy transfer (FRET). Varying the cyanide concentration in the range of 3 to 100 μM linearly changed the fluorescence intensity of Lys-AuNCs (R^2 = 0.9957). The reproducibility for the quantitative analysis of

cyanide was excellent. Another example of ratiometric sensing is provided by Gao et al., who synthetized aprotinin-encapsulated gold nanoclusters (Ap-AuNCs) as a probe for proteases and heavy metals. As shown in Figure 8, Ap-AuNCs mixed with proteinases were found to exhibit decreased fluorescence intensity; the decrease was most significant for trypsin and the detection limit for trypsin was calculated to be 10.18 μm/mL [134].

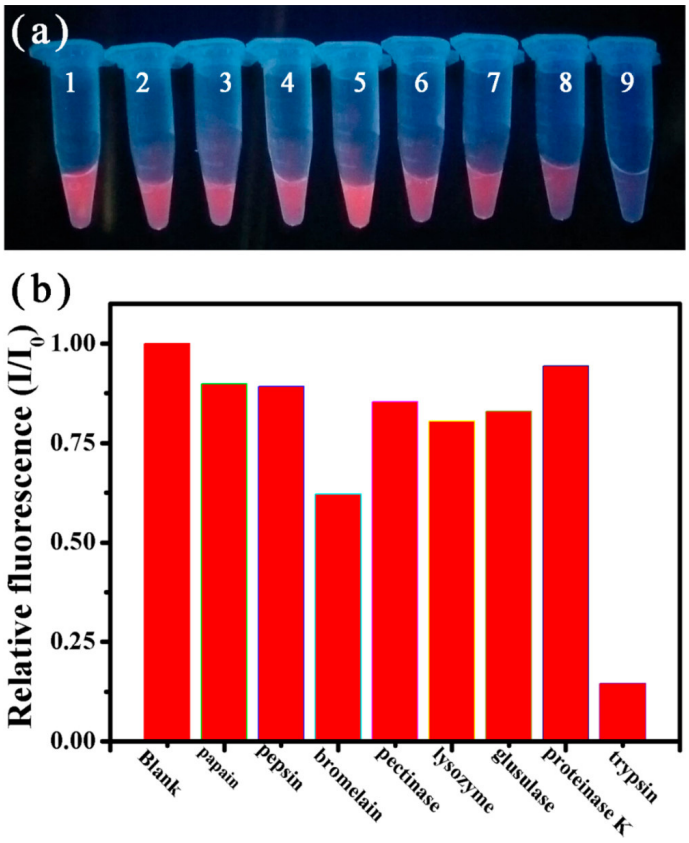

Figure 8. (**a**) Digital photographs of aqueous Ap-AuNC solutions in the presence of different proteases under UV illumination (from 1 to 9: blank, papain, pepsin, pectinase, lysozyme, glusulase, proteinase K, bromelain, and trypsin). (**b**) Relative fluorescence intensity of Ap-Au NCs (I/I_0, where I and I_0 are the fluorescence intensity of AuNCs in the presence and absence of trypsin at 640 nm, respectively) in the presence and absence of various proteases (λ_{ex} = 550 nm, λ_{em} = 640 nm). Reprinted with permission from Ref. [134]. Copyright 2018 American Chemical Society.

The first group to show that BSA-AuNC can be used as a sensor for Hg^{2+} was Xie et al. [135]. Ap-AuNCs were also investigated as a probe for heavy metal. Among 12 common cations, the addition of Hg^{2+} and Cu^{2+} resulted in an obvious decrease in fluorescence intensity [134]. These results are in good agreement with other previously published data [136,137]. Similarly, β-lactoglobulin-AuNCs also were reported to exhibit high sensitivity and selectivity for the detection of Hg^{2+} in aqueous media and were used as fluorescence sensors to determine the concentration of Hg^{2+} with high sensitivity in urine, beverages, and serum samples [138].

Ligand-protected AuNCs reveal great potential in the field of oncology—including their use in tumor photodynamic therapy, photothermal therapy, and combination therapy—due to the fact that they exhibit well-proven tumor penetration and accumulation ability. Raju et al. used PSP001 (a polysaccharide isolated from pomegranate peel) coupled with L-cysteine (Y) as the ligand for AuNCs synthesis. PSP001 exhibits anticancer, antioxidant, and antimetastatic activity. The resultant PSP-Y-AuNCs exhibited pH-sensitive fluorescence emission and could be used for real-time fluorescence imaging of cancer

tissues [139]. Dutta et al. employed methylene blue as a photosensitizer, incorporating it onto AuNCs stabilized by a glycoprotein, mucin, which enabled the complex to cross complex barriers and enhanced its biocompatibility and ability for tissue penetration and delivery. This facilitated the effective absorption and accumulation of this complex within HeLa cells. Upon exposure to 640 nm light, the apoptosis of HeLa cells was induced [140]. The resulting confocal microscopy images are shown in Figure 9.

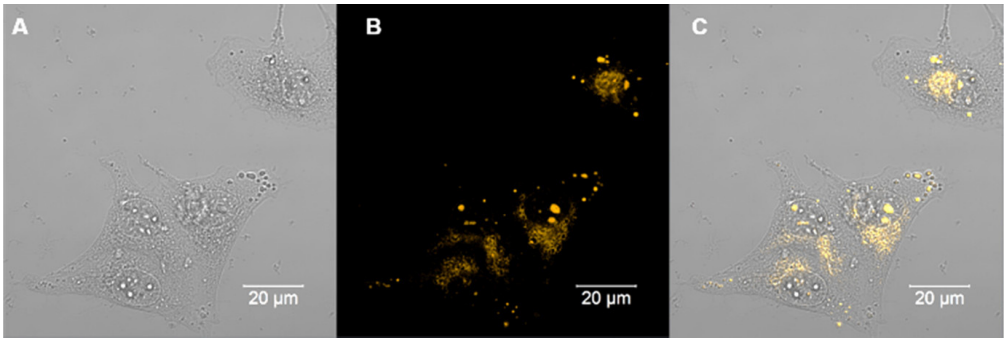

Figure 9. Images of HeLa cells obtained by confocal microscopy: (**A**) bright-field, (**B**) fluorescence, and (**C**) overlay images, respectively, after treatment with MB-loaded Au NC–mucin NPs. Reprinted (adapted) with permission from Ref. [140]. Copyright 2019 American Chemical Society.

AuNCs can also directly participate in photodynamic therapy as photosensitizers. The Au_{25} nanoclusters exhibit a long lifetime of electronically excited states, which enables the Au_{25}NCs to efficiently generate singlet oxygen under irradiation at appropriate wavelengths. When Poderys at al. irradiated human breast cancer cells MCF-7 and MDA-MB-231 containing BSA-AuNCs with ultraviolet light, their survival rates decreased to 13% and 50%, respectively [141].

Here, we have presented only a few examples of various biomedical applications of protein-protected AuNCs. The evidence presented thus far supports the idea that their applications are very exciting and worth exploring in the future. More examples can be found in excellent reviews published to this date [142–144].

9. Conclusions

This concise paper summarizes the current state of mechanistic and applied studies (as well as challenges) on using proteins and peptides as templates for the synthesis of luminescent gold nanoclusters.

Following the original discovery of the one-pot synthetic pathway to albumin-protected BSA-AuNCs by Xie et al., numerous studies have highlighted the importance of particular chemical and macromolecular features of the proteinaceous co-substrates. The picture emerging from these works is both fascinating and intricate: a serendipitously fruitful interplay of reducing, electron-donating, Au-binding, nanoparticle-protecting, and biocompatibility-promoting properties of these proteins make them excellent reagents and building blocks of the eventual product—a stable luminescent protein–AuNC nanocluster conjugate with many potential biomedical applications. With our deepening understanding of the roles played in this process by local (e.g., chemistry of individual amino acid side chains) and global (protein molecule structure, size, and dynamics) factors, it is tempting to anticipate even more intelligently designed application-focused protein–AuNC hybrid systems. While one of the benefits of using BSA for the synthesis of these conjugates is the low cost of the protein component, the genetic or chemical manipulation of the amino acid sequence will facilitate the fine-tuning of the optical properties and biocompatibility of these conjugates.

It is also crucial to gather more information about the changes in the structure of proteins resulting from the incorporation of nanoclusters. One should note that the protein unfolding could in fact impact the accessibility of the clusters embedded within it, as well as the accessibility of certain amino acid residues.

The protein-protected nanoclusters are extremely challenging systems to study and there remain several mechanistic and application-related challenges that need to be addressed in the coming years [145]. For example, one must consider the existence of the mixture of Au oxidation states, multiple binding sites, and resulting conformational changes in the protein, differences in the local environment of luminescent centers, and the size distribution of AuNCs. Therefore, further investigation and the independent repetition of the experiments are essential to establish a clearer understanding of the protein's role within these systems and to standardize approaches for studying protein-protected nanoclusters across varied conditions. The unification of the information provided in the literature will be essential for formulating further research questions in this field. The fascinating range of potential applications of protein–AuNCs systems are well worth these efforts, however.

Funding: This work was supported by the National Science Centre of Poland, grant no. 2017/25/B/ST5/02599.

Conflicts of Interest: The authors declare no conflicts of interest.

References

1. Qian, H.; Zhu, M.; Wu, Z.; Jin, R. Quantum Sized Gold Nanoclusters with Atomic Precision. *Acc. Chem. Res.* **2012**, *45*, 1470–1479. [CrossRef]
2. Bian, P.; Zhou, J.; Liu, Y.; Ma, Z. One-Step Fabrication of Intense Red Fluorescent Gold Nanoclusters and Their Application in Cancer Cell Imaging. *Nanoscale* **2013**, *5*, 6161. [CrossRef] [PubMed]
3. Ding, C.; Xu, Y.; Zhao, Y.; Zhong, H.; Luo, X. Fabrication of BSA@AuNC-Based Nanostructures for Cell Fluoresce Imaging and Target Drug Delivery. *ACS Appl. Mater. Interfaces* **2018**, *10*, 8947–8954. [CrossRef] [PubMed]
4. Durante, N.; Fortunelli, A.; Broyer, M.; Stener, M. Optical Properties of Au Nanoclusters from TD-DFT Calculations. *J. Phys. Chem. C* **2011**, *115*, 6277–6282. [CrossRef]
5. Zheng, J.; Zhang, C.; Dickson, R.M. Highly Fluorescent, Water-Soluble, Size-Tunable Gold Quantum Dots. *Phys. Rev. Lett.* **2004**, *93*, 077402. [CrossRef]
6. Zheng, J.; Nicovich, P.R.; Dickson, R.M. Highly Fluorescent Noble-Metal Quantum Dots. *Annu. Rev. Phys. Chem.* **2007**, *58*, 409–431. [CrossRef]
7. Kang, X.; Chong, H.; Zhu, M. $Au_{25}(SR)_{18}$: The Captain of the Great Nanocluster Ship. *Nanoscale* **2018**, *10*, 10758–10834. [CrossRef]
8. Raut, S.; Chib, R.; Rich, R.; Shumilov, D.; Gryczynski, Z.; Gryczynski, I. Polarization Properties of Fluorescent BSA Protected Au_{25} Nanoclusters. *Nanoscale* **2013**, *5*, 3441. [CrossRef]
9. Zhu, M.; Aikens, C.M.; Hollander, F.J.; Schatz, G.C.; Jin, R. Correlating the Crystal Structure of A Thiol-Protected Au_{25} Cluster and Optical Properties. *J. Am. Chem. Soc.* **2008**, *130*, 5883–5885. [CrossRef]
10. Xu, S.; Yang, H.; Zhao, K.; Li, J.; Mei, L.; Xie, Y.; Deng, A. Simple and Rapid Preparation of Orange-Yellow Fluorescent Gold Nanoclusters Using DL -Homocysteine as a Reducing/Stabilizing Reagent and Their Application in Cancer Cell Imaging. *RSC Adv.* **2015**, *5*, 11343–11348. [CrossRef]
11. Bai, Y.; Shu, T.; Su, L.; Zhang, X. Fluorescent Gold Nanoclusters for Biosensor and Bioimaging Application. *Crystals* **2020**, *10*, 357. [CrossRef]
12. Liu, J.-M.; Yan, X.-P. Competitive Aptamer Bioassay for Selective Detection of Adenosine Triphosphate Based on Metal-Paired Molecular Conformational Switch and Fluorescent Gold Nanoclusters. *Biosens. Bioelectron.* **2012**, *36*, 135–141. [CrossRef] [PubMed]
13. Upadhyay, Y.; Kumar, R.; Sahoo, S.K. Developing a Cost-Effective Bioassay to Detect Alkaline Phosphatase Activity and Generating White Light Emission from a Single Nano-Assembly by Conjugating Vitamin B_6 Cofactors with Lysozyme-Stabilized Fluorescent Gold Nanoclusters. *ACS Sustain. Chem. Eng.* **2020**, *8*, 4107–4113. [CrossRef]
14. Wen, F.; Dong, Y.; Feng, L.; Wang, S.; Zhang, S.; Zhang, X. Horseradish Peroxidase Functionalized Fluorescent Gold Nanoclusters for Hydrogen Peroxide Sensing. *Anal. Chem.* **2011**, *83*, 1193–1196. [CrossRef]
15. Xu, Y.; Yang, X.; Zhu, S.; Dou, Y. Selectively Fluorescent Sensing of Cu2+ Based on Lysine-Functionalized Gold Nanoclusters. *Colloids Surf. A Physicochem. Eng. Asp.* **2014**, *450*, 115–120. [CrossRef]

16. Zhang, H.; Liu, Q.; Wang, T.; Yun, Z.; Li, G.; Liu, J.; Jiang, G. Facile Preparation of Glutathione-Stabilized Gold Nanoclusters for Selective Determination of Chromium (III) and Chromium (VI) in Environmental Water Samples. *Anal. Chim. Acta* **2013**, *770*, 140–146. [CrossRef]
17. Liu, M.; Tang, F.; Yang, Z.; Xu, J.; Yang, X. Recent Progress on Gold-Nanocluster-Based Fluorescent Probe for Environmental Analysis and Biological Sensing. *J. Anal. Methods Chem.* **2019**, *2019*, 1095148. [CrossRef]
18. Yahia-Ammar, A.; Sierra, D.; Mérola, F.; Hildebrandt, N.; Le Guével, X. Self-Assembled Gold Nanoclusters for Bright Fluorescence Imaging and Enhanced Drug Delivery. *ACS Nano* **2016**, *10*, 2591–2599. [CrossRef]
19. Liu, J.; Duchesne, P.N.; Yu, M.; Jiang, X.; Ning, X.; Vinluan, R.D.; Zhang, P.; Zheng, J. Luminescent Gold Nanoparticles with Size-Independent Emission. *Angew. Chem. Int. Ed.* **2016**, *55*, 8894–8898. [CrossRef]
20. Guo, Y.; Shen, F.; Cheng, Y.; Xie, Y.; Yu, H.; Yao, W.; Li, H.-W.; Qian, H.; Pei, R. The Light-up Fluorescence of AgNCs in a "DNA Bulb". *Nanoscale* **2018**, *10*, 11517–11523. [CrossRef]
21. Xie, Y.; Liu, Y.; Yang, J.; Liu, Y.; Hu, F.; Zhu, K.; Jiang, X. Gold Nanoclusters for Targeting Methicillin-Resistant *Staphylococcus Aureus* In Vivo. *Angew. Chem. Int. Ed.* **2018**, *57*, 3958–3962. [CrossRef] [PubMed]
22. Gröhn, F.; Bauer, B.; Akpalu, Y.; Jackson, C.; Amis, E. Dendrimer Templates for the Formation of Gold Nanoclusters. *Macromolecules* **2000**, *33*, 6042–6050. [CrossRef]
23. Tran, M.L.; Zvyagin, A.V.; Plakhotnik, T. Synthesis and Spectroscopic Observation of Dendrimer-Encapsulated Gold Nanoclusters. *Chem. Commun.* **2006**, *22*, 2400–2401. [CrossRef]
24. Zhao, Y.; Zhou, H.; Antoine, R.; Zhang, S. Polymer- and Dendrimer-Protected Metal Nanoclusters. In *Luminescent Metal Nanoclusters*; Elsevier: Amsterdam, The Netherlands, 2022; pp. 223–249. ISBN 978-0-323-88657-4.
25. Tsunoyama, H.; Sakurai, H.; Negishi, Y.; Tsukuda, T. Size-Specific Catalytic Activity of Polymer-Stabilized Gold Nanoclusters for Aerobic Alcohol Oxidation in Water. *J. Am. Chem. Soc.* **2005**, *127*, 9374–9375. [CrossRef]
26. Biswas, A.; Banerjee, S.; Gart, E.V.; Nagaraja, A.T.; McShane, M.J. Gold Nanocluster Containing Polymeric Microcapsules for Intracellular Ratiometric Fluorescence Biosensing. *ACS Omega* **2017**, *2*, 2499–2506. [CrossRef]
27. Deepagan, V.G.; Leiske, M.N.; Fletcher, N.L.; Rudd, D.; Tieu, T.; Kirkwood, N.; Thurecht, K.J.; Kempe, K.; Voelcker, N.H.; Cifuentes-Rius, A. Engineering Fluorescent Gold Nanoclusters Using Xanthate-Functionalized Hydrophilic Polymers: Toward Enhanced Monodispersity and Stability. *Nano Lett.* **2021**, *21*, 476–484. [CrossRef]
28. Xu, J.; Li, J.; Zhong, W.; Wen, M.; Sukhorukov, G.; Shang, L. The Density of Surface Ligands Regulates the Luminescence of Thiolated Gold Nanoclusters and Their Metal Ion Response. *Chin. Chem. Lett.* **2021**, *32*, 2390–2394. [CrossRef]
29. Kwak, K.; Kumar, S.S.; Pyo, K.; Lee, D. Ionic Liquid of a Gold Nanocluster: A Versatile Matrix for Electrochemical Biosensors. *ACS Nano* **2014**, *8*, 671–679. [CrossRef]
30. Bera, N.; Kiran Nandi, P.; Hazra, R.; Sarkar, N. Oligo. *J. Photochem. Photobiol. A Chem.* **2023**, *437*, 114471. [CrossRef]
31. Gu, Y.; Wen, Q.; Kuang, Y.; Tang, L.; Jiang, J. Peptide-Templated Gold Nanoclusters as a Novel Label-Free Biosensor for the Detection of Protease Activity. *RSC Adv.* **2014**, *4*, 13753–13756. [CrossRef]
32. Xie, J.; Zheng, Y.; Ying, J. Protein-Directed Synthesis of Highly Fluorescent Gold Nanoclusters. *J. Am. Chem. Soc.* **2009**, *131*, 888–889. [CrossRef] [PubMed]
33. Qing, T.; He, X.; He, D.; Qing, Z.; Wang, K.; Lei, Y.; Liu, T.; Tang, P.; Li, Y. Oligonucleotide-Templated Rapid Formation of Fluorescent Gold Nanoclusters and Its Application for Hg^{2+} Ions Sensing. *Talanta* **2016**, *161*, 170–176. [CrossRef] [PubMed]
34. Liu, G.; Shao, Y.; Ma, K.; Cui, Q.; Wu, F.; Xu, S. Synthesis of DNA-Templated Fluorescent Gold Nanoclusters. *Gold Bull.* **2012**, *45*, 69–74. [CrossRef]
35. Kennedy, T.A.C.; MacLean, J.L.; Liu, J. Blue Emitting Gold Nanoclusters Templated by Poly-Cytosine DNA at Low pH and Poly-Adenine DNA at Neutral pH. *Chem. Commun.* **2012**, *48*, 6845. [CrossRef]
36. Liu, G.; Shao, Y.; Wu, F.; Xu, S.; Peng, J.; Liu, L. DNA-Hosted Fluorescent Gold Nanoclusters: Sequence-Dependent Formation. *Nanotechnology* **2013**, *24*, 015503. [CrossRef]
37. Yabu, H. One-Pot Synthesis of Blue Light-Emitting Au Nanoclusters and Formation of Photo-Patternable Composite Films. *Chem. Commun.* **2011**, *47*, 1196–1197. [CrossRef]
38. Dridi, N.; Jin, Z.; Perng, W.; Mattoussi, H. Probing Protein Corona Formation around Gold Nanoparticles: Effects of Surface Coating. *ACS Nano* **2024**, *18*, 8649–8662. [CrossRef]
39. Gombár, G.; Simon, P.; Ungor, D.; Szatmári, I.; Csapó, E. Histidinehydroxamic Acid as New Biomolecule to Produce Molecular-like Fluorescent Gold Nanoclusters: Possible Mechanisms for Metal Ion Sensing. *J. Mol. Liq.* **2023**, *387*, 122597. [CrossRef]
40. Gombár, G.; Ungor, D.; Samu, G.F.; Dömötör, O.; Csapó, E. Synthesis and Characterization of Novel Blue-Emitting Nicotinamide-Gold Nanoclusters with "Chain-Breaker" Antioxidant Property. *J. Mol. Liq.* **2022**, *359*, 119372. [CrossRef]
41. Jiang, J.; Conroy, C.V.; Kvetny, M.M.; Lake, G.J.; Padelford, J.W.; Ahuja, T.; Wang, G. Oxidation at the Core–Ligand Interface of Au Lipoic Acid Nanoclusters That Enhances the Near-IR Luminescence. *J. Phys. Chem. C* **2014**, *118*, 20680–20687. [CrossRef]
42. Feng, J.-J.; Huang, H.; Chen, W.-J.; Chen, J.-R.; Lin, H.-J.; Wang, A.-J. Sensitive Detection of Mercury (II) Ion Using Water-Soluble Captopril-Stabilized Fluorescent Gold Nanoparticles. *Mater. Sci. Eng. C* **2013**, *33*, 2664–2668. [CrossRef] [PubMed]

43. Shang, L.; Dörlich, R.M.; Brandholt, S.; Schneider, R.; Trouillet, V.; Bruns, M.; Gerthsen, D.; Nienhaus, G.U. Facile Preparation of Water-Soluble Fluorescent Gold Nanoclusters for Cellular Imaging Applications. *Nanoscale* **2011**, *3*, 2009. [CrossRef] [PubMed]
44. Zheng, Y.; Liu, W.; Chen, Y.; Li, C.; Jiang, H.; Wang, X. Conjugating Gold Nanoclusters and Antimicrobial Peptides: From Aggregation-Induced Emission to Antibacterial Synergy. *J. Colloid Interface Sci.* **2019**, *546*, 1–10. [CrossRef] [PubMed]
45. Cui, M.; Ono, M.; Watanabe, H.; Kimura, H.; Liu, B.; Saji, H. Smart Near-Infrared Fluorescence Probes with Donor–Acceptor Structure for in Vivo Detection of β-Amyloid Deposits. *J. Am. Chem. Soc.* **2014**, *136*, 3388–3394. [CrossRef]
46. Goswami, N.; Saha, R.; Pal, S.K. Protein-Assisted Synthesis Route of Metal Nanoparticles: Exploration of Key Chemistry of the Biomolecule. *J. Nanopart. Res.* **2011**, *13*, 5485–5495. [CrossRef]
47. Yue, Y.; Liu, T.-Y.; Li, H.-W.; Liu, Z.; Wu, Y. Microwave-Assisted Synthesis of BSA-Protected Small Gold Nanoclusters and Their Fluorescence-Enhanced Sensing of Silver(i) Ions. *Nanoscale* **2012**, *4*, 2251. [CrossRef]
48. Zhang, J.; Yuan, Y.; Liang, G.; Arshad, M.N.; Albar, H.A.; Sobahi, T.R.; Yu, S.-H. A Microwave-Facilitated Rapid Synthesis of Gold Nanoclusters with Tunable Optical Properties for Sensing Ions and Fluorescent Ink. *Chem. Commun.* **2015**, *51*, 10539–10542. [CrossRef]
49. Hsu, N.-Y.; Lin, Y.-W. Microwave-Assisted Synthesis of Bovine Serum Albumin–Gold Nanoclusters and Their Fluorescence-Quenched Sensing of Hg^{2+} Ions. *New J. Chem.* **2016**, *40*, 1155–1161. [CrossRef]
50. Hada, A.-M.; Zetes, M.; Focsan, M.; Astilean, S.; Craciun, A.-M. Photoluminescent Histidine-Stabilized Gold Nanoclusters as Efficient Sensors for Fast and Easy Visual Detection of Fe Ions in Water Using Paper-Based Portable Platform. *Int. J. Mol. Sci.* **2022**, *23*, 12410. [CrossRef]
51. Retnakumari, A.; Setua, S.; Menon, D.; Ravindran, P.; Muhammed, H.; Pradeep, T.; Nair, S.; Koyakutty, M. Molecular-Receptor-Specific, Non-Toxic, near-Infrared-Emitting Au Cluster-Protein Nanoconjugates for Targeted Cancer Imaging. *Nanotechnology* **2010**, *21*, 055103. [CrossRef]
52. Volden, S.; Lystvet, S.M.; Halskau, Ø.; Glomm, W.R. Generally Applicable Procedure for in Situ Formation of Fluorescent Protein-Gold Nanoconstructs. *RSC Adv.* **2012**, *2*, 11704. [CrossRef]
53. Lu, D.; Liu, L.; Li, F.; Shuang, S.; Li, Y.; Choi, M.M.F.; Dong, C. Lysozyme-Stabilized Gold Nanoclusters as a Novel Fluorescence Probe for Cyanide Recognition. *Spectrochim. Acta Part A Mol. Biomol. Spectrosc.* **2014**, *121*, 77–80. [CrossRef] [PubMed]
54. Alkudaisi, N.; Russell, B.A.; Birch, D.J.S.; Chen, Y. Lysozyme Encapsulated Gold Nanoclusters for Probing the Early Stage of Lysozyme Aggregation under Acidic Conditions. *J. Photochem. Photobiol. B Biol.* **2019**, *197*, 111540. [CrossRef]
55. Kawasaki, H.; Hamaguchi, K.; Osaka, I.; Arakawa, R. pH-Dependent Synthesis of Pepsin-Mediated Gold Nanoclusters with Blue Green and Red Fluorescent Emission. *Adv. Funct. Mater.* **2011**, *21*, 3508–3515. [CrossRef]
56. Liu, J.-M.; Chen, J.-T.; Yan, X.-P. Near Infrared Fluorescent Trypsin Stabilized Gold Nanoclusters as Surface Plasmon Enhanced Energy Transfer Biosensor and In Vivo Cancer Imaging Bioprobe. *Anal. Chem.* **2013**, *85*, 3238–3245. [CrossRef]
57. West, A.L.; Griep, M.H.; Cole, D.P.; Karna, S.P. Gold Nanocluster DNase 1 Hybrid Materials: An Efficient Method for DNA Contamination Sensing. *IEEE Nanotechnol. Mag.* **2015**, *9*, 25–30. [CrossRef]
58. Li, H.; Zhu, W.; Wan, A.; Liu, L. The Mechanism and Application of the Protein-Stabilized Gold Nanocluster Sensing System. *Analyst* **2017**, *142*, 567–581. [CrossRef]
59. Hu, L.; Han, S.; Parveen, S.; Yuan, Y.; Zhang, L.; Xu, G. Highly Sensitive Fluorescent Detection of Trypsin Based on BSA-Stabilized Gold Nanoclusters. *Biosens. Bioelectron.* **2012**, *32*, 297–299. [CrossRef]
60. Zhang, S.; Chen, C.; Qin, X.; Zhang, Q.; Liu, J.; Zhu, J.; Gao, Y.; Li, L.; Huang, W. Ultrasensitive Detection of Trypsin Activity and Inhibitor Screening Based on the Electron Transfer between Phosphorescence Copper Nanocluster and Cytochrome c. *Talanta* **2018**, *189*, 92–99. [CrossRef]
61. Wacławska, M.; Nieznańska, H.; Dzwolak, W. Enzymatic Digestion of Luminescent Albumin-Stabilized Gold Nanoclusters under Anaerobic Conditions: Clues to the Quenching Mechanism. *J. Mater. Chem. C* **2022**, *10*, 3775–3783. [CrossRef]
62. Das, T.; Ghosh, P.; Shanavas, M.S.; Maity, A.; Mondal, S.; Purkayastha, P. Protein-Templated Gold Nanoclusters: Size Dependent Inversion of Fluorescence Emission in the Presence of Molecular Oxygen. *Nanoscale* **2012**, *4*, 6018. [CrossRef] [PubMed]
63. Liu, W.; Zhang, H.; Dong, X.; Sun, Y. Composite of Gold Nanoclusters and Basified Human Serum Albumin Significantly Boosts the Inhibition of Alzheimer's β-Amyloid by Photo-Oxygenation. *Acta Biomater.* **2022**, *144*, 157–167. [CrossRef] [PubMed]
64. Liu, C.-L.; Wu, H.-T.; Hsiao, Y.-H.; Lai, C.-W.; Shih, C.-W.; Peng, Y.-K.; Tang, K.-C.; Chang, H.-W.; Chien, Y.-C.; Hsiao, J.-K.; et al. Insulin-Directed Synthesis of Fluorescent Gold Nanoclusters: Preservation of Insulin Bioactivity and Versatility in Cell Imaging. *Angew. Chem. Int. Ed.* **2011**, *50*, 7056–7060. [CrossRef]
65. Ghosh, S.; Bhamore, J.R.; Malek, N.I.; Murthy, Z.V.P.; Kailasa, S.K. Trypsin Mediated One-Pot Reaction for the Synthesis of Red Fluorescent Gold Nanoclusters: Sensing of Multiple Analytes (Carbidopa, Dopamine, Cu^{2+}, Co^{2+} and Hg^{2+} Ions). *Spectrochim. Acta Part A Mol. Biomol. Spectrosc.* **2019**, *215*, 209–217. [CrossRef]
66. Chen, Y.; Wang, Y.; Wang, C.; Li, W.; Zhou, H.; Jiao, H.; Lin, Q.; Yu, C. Papain-Directed Synthesis of Luminescent Gold Nanoclusters and the Sensitive Detection of Cu^{2+}. *J. Colloid Interface Sci.* **2013**, *396*, 63–68. [CrossRef]

67. Guével, X.L.; Daum, N.; Schneider, M. Synthesis and Characterization of Human Transferrin-Stabilized Gold Nanoclusters. *Nanotechnology* **2011**, *22*, 275103. [CrossRef]
68. Xavier, P.L.; Chaudhari, K.; Verma, P.K.; Pal, S.K.; Pradeep, T. Luminescent Quantum Clusters of Gold in Transferrin Family Protein, Lactoferrin Exhibiting FRET. *Nanoscale* **2010**, *2*, 2769. [CrossRef]
69. Li, Y.; Peng, W.; You, X. Determination of Dopamine by Exploiting the Catalytic Effect of Hemoglobin–Stabilized Gold Nanoclusters on the Luminol–$NaIO_4$ Chemiluminescence System. *Microchim. Acta* **2017**, *184*, 3539–3545. [CrossRef]
70. Tan, S.-H.; Yougbaré, S.; Chu, H.-L.; Kuo, T.-R.; Cheng, T.-M. Hemoglobin-Conjugated Gold Nanoclusters for Qualitative Analysis of Haptoglobin Phenotypes. *Polymers* **2020**, *12*, 2242. [CrossRef]
71. Cun, X.; Jansman, M.M.T.; Liu, X.; Boureau, V.; Thulstrup, P.W.; Hosta-Rigau, L. Hemoglobin-Stabilized Gold Nanoclusters Displaying Oxygen Transport Ability, Self-Antioxidation, Auto-Fluorescence Properties and Long-Term Storage Potential. *RSC Adv.* **2023**, *13*, 15540–15553. [CrossRef]
72. Ling, S.; Liang, H.; Li, Z.; Ma, L.; Yao, J.; Shao, Z.; Chen, X. Soy Protein-Directed One-Pot Synthesis of Gold Nanomaterials and Their Functional Conductive Devices. *J. Mater. Chem. B* **2016**, *4*, 3643–3650. [CrossRef] [PubMed]
73. Shi, H.; Ou, M.Y.; Cao, J.P.; Chen, G.F. Synthesis of Ovalbumin-Stabilized Highly Fluorescent Gold Nanoclusters and Their Application as an Hg^{2+} Sensor. *RSC Adv.* **2015**, *5*, 86740–86745. [CrossRef]
74. Yarramala, D.S.; Baksi, A.; Pradeep, T.; Rao, C.P. Green Synthesis of Protein-Protected Fluorescent Gold Nanoclusters (AuNCs): Reducing the Size of AuNCs by Partially Occupying the Ca^{2+} Site by La^{3+} in Apo-α-Lactalbumin. *ACS Sustain. Chem. Eng.* **2017**, *5*, 6064–6069. [CrossRef]
75. Li, X.; Qiao, J.; Li, Z.; Qi, L. Dual Protein Ligand-Modified Gold Nanoclusters for Selective Detection of Serum Sodium Copper Chlorophyllin. *Spectrochim. Acta Part A Mol. Biomol. Spectrosc.* **2020**, *243*, 118798. [CrossRef]
76. Tang, Z.; Chen, F.; Wang, D.; Xiong, D.; Yan, S.; Liu, S.; Tang, H. Fabrication of Avidin-Stabilized Gold Nanoclusters with Dual Emissions and Their Application in Biosensing. *J. Nanobiotechnol.* **2022**, *20*, 306. [CrossRef]
77. Zhang, X.; Chen, M.; Zhang, Y.; Hou, Y.; Wu, Y.; Yao, M.; Li, L.; Shi, L.; Liu, T.; Hu, B.; et al. Monoclonal-Antibody-Templated Gold Nanoclusters for HER2 Receptors Targeted Fluorescence Imaging. *ACS Appl. Bio Mater.* **2020**, *3*, 7061–7066. [CrossRef]
78. Kundu, A.; Park, B.; Ray, C.; Oh, J.; Jun, S.C. Environmentally Benign and Cost-Effective Synthesis of Water Soluble Red Light Emissive Gold Nanoclusters: Selective and Ultra-Sensitive Detection of Mercuric Ions. *New J. Chem.* **2019**, *43*, 900–906. [CrossRef]
79. Wang, M.; Chen, J.; Jiang, S.; Nie, Y.; Su, X. Rapid Synthesis of Dual Proteins Co-Functionalized Gold Nanoclusters for Ratiometric Fluorescence Sensing of Polynucleotide Kinase Activity. *Sens. Actuators B Chem.* **2021**, *329*, 129200. [CrossRef]
80. Yang, X.; Luo, Y.; Zhuo, Y.; Feng, Y.; Zhu, S. Novel Synthesis of Gold Nanoclusters Templated with L-Tyrosine for Selective Analyzing Tyrosinase. *Anal. Chim. Acta* **2014**, *840*, 87–92. [CrossRef]
81. Retnakumari, A.; Jayasimhan, J.; Chandran, P.; Menon, D.; Nair, S.; Mony, U.; Koyakutty, M. CD33 Monoclonal Antibody Conjugated Au Cluster Nano-Bioprobe for Targeted Flow-Cytometric Detection of Acute Myeloid Leukaemia. *Nanotechnology* **2011**, *22*, 285102. [CrossRef]
82. Storm, A.J.; Chen, J.H.; Ling, X.S.; Zandbergen, H.W.; Dekker, C. Electron-Beam-Induced Deformations of SiO_2 Nanostructures. *J. Appl. Phys.* **2005**, *98*, 014307. [CrossRef]
83. Furuya, K. Nanofabrication by Advanced Electron Microscopy Using Intense and Focused Beam. *Sci. Technol. Adv. Mater.* **2008**, *9*, 014110. [CrossRef]
84. Ahmad, N.; Le Bouar, Y.; Ricolleau, C.; Alloyeau, D. Growth of Dendritic Nanostructures by Liquid-Cell Transmission Electron Microscopy: A Reflection of the Electron-Irradiation History. *Adv. Struct. Chem. Imag.* **2016**, *2*, 9. [CrossRef]
85. Ostruszka, R.; Zoppellaro, G.; Tomanec, O.; Pinkas, D.; Filimonenko, V.; Šišková, K. Evidence of Au(II) and Au(0) States in Bovine Serum Albumin-Au Nanoclusters Revealed by CW-EPR/LEPR and Peculiarities in HR-TEM/STEM Imaging. *Nanomaterials* **2022**, *12*, 1425. [CrossRef] [PubMed]
86. Madhu, M.; Tseng, W.-B.; Chou, Y.-S.; Krishna Kumar, A.S.; Lu, C.-Y.; Chang, P.-L.; Tseng, W.-L. Peptide-Directed Synthesis of Aggregation-Induced Emission Enhancement-Active Gold Nanoclusters for Single- and Two-Photon Imaging of Lysosome and Expressed Avβ3 Integrin Receptors. *Anal. Chem.* **2024**, *96*, 9007–9015. [CrossRef] [PubMed]
87. Csapó, E.; Ungor, D.; Kele, Z.; Baranyai, P.; Deák, A.; Juhász, Á.; Janovák, L.; Dékány, I. Influence of pH and Aurate/Amino Acid Ratios on the Tuneable Optical Features of Gold Nanoparticles and Nanoclusters. *Colloids Surf. A Physicochem. Eng. Asp.* **2017**, *532*, 601–608. [CrossRef]
88. Yang, X.; Shi, M.; Zhou, R.; Chen, X.; Chen, H. Blending of HAuCl4 and Histidine in Aqueous Solution: A Simple Approach to the Au10 Cluster. *Nanoscale* **2011**, *3*, 2596. [CrossRef]
89. Xu, Y.; Sherwood, J.; Qin, Y.; Crowley, D.; Bonizzoni, M.; Bao, Y. The Role of Protein Characteristics in the Formation and Fluorescence of Au Nanoclusters. *Nanoscale* **2014**, *6*, 1515–1524. [CrossRef]
90. Rajamanikandan, R.; Ilanchelian, M. Protein-Localized Bright-Red Fluorescent Gold Nanoclusters as Cyanide-Selective Colorimetric and Fluorometric Nanoprobes. *ACS Omega* **2018**, *3*, 14111–14118. [CrossRef]

91. Kluz, M.; Nieznańska, H.; Dec, R.; Dzięcielewski, I.; Niżyński, B.; Ścibisz, G.; Dzwolak, W. Revisiting the Conformational State of Albumin Conjugated to Gold Nanoclusters: A Self-Assembly Pathway to Giant Superstructures Unraveled. *PLoS ONE* **2019**, *14*, 0218975. [CrossRef]
92. Sen, P.; Ahmad, B.; Khan, R.H. Formation of a Molten Globule like State in Bovine Serum Albumin at Alkaline pH. *Eur. Biophys. J.* **2008**, *37*, 1303–1308. [CrossRef] [PubMed]
93. Baksi, A.; Xavier, P.L.; Chaudhari, K.; Goswami, N.; Pal, S.K.; Pradeep, T. Protein-Encapsulated Gold Cluster Aggregates: The Case of Lysozyme. *Nanoscale* **2013**, *5*, 2009. [CrossRef]
94. Shamsipur, M.; Babaee, E.; Gholivand, M.-B.; Molaabasi, F.; Mousavi, F.; Barati, A.; Hajipour Verdom, B.; Shojaedin-Givi, B.; Naderi-Manesh, H. Bright Green Light-Emitting Gold Nanoclusters Confined in Insulin as Selective Fluorescent Switch Probes for Sensing and Imaging of Copper Ions and Glutathione. *ACS Appl. Nano Mater.* **2023**, *6*, 5939–5951. [CrossRef]
95. Kaumbekova, S.; Sakaguchi, N.; Shah, D.; Umezawa, M. Effect of Gold Nanoparticles on the Conformation of Bovine Serum Albumin: Insights from CD Spectroscopic Analysis and Molecular Dynamics Simulations. *ACS Omega* **2024**, *9*, 49283–49292. [CrossRef] [PubMed]
96. Varga, N.; Hornok, V.; Sebők, D.; Dékány, I. Comprehensive Study on the Structure of the BSA from Extended-to Aged Form in Wide (2–12) pH Range. *Int. J. Biol. Macromol.* **2016**, *88*, 51–58. [CrossRef]
97. Yu, Y.; Luo, Z.; Teo, C.S.; Tan, Y.N.; Xie, J. Tailoring the Protein Conformation to Synthesize Different-Sized Gold Nanoclusters. *Chem. Commun.* **2013**, *49*, 9740. [CrossRef]
98. Michnik, A. Thermal stability of bovine serum albumin DSC study. *J. Therm. Anal. Calorim.* **2003**, *71*, 509–519. [CrossRef]
99. Oleszko, A.; Hartwich, J.; Gąsior-Głogowska, M.; Olsztyńska-Janus, S. Changes of Albumin Secondary Structure after Palmitic Acid Binding. FT-IR Spectroscopic Study. *Acta Bioeng. Biomech.* **2018**, *20*, 59–64.
100. Andrýsková, P.; Šišková, K.M.; Michetschlägerová, Š.; Jiráková, K.; Kubala, M.; Jirák, D. The Effect of Fatty Acids and BSA Purity on Synthesis and Properties of Fluorescent Gold Nanoclusters. *Nanomaterials* **2020**, *10*, 343. [CrossRef]
101. Tan, Y.N.; Lee, J.Y.; Wang, D.I. Uncovering the Design Rules for Peptide Synthesis of Metal Nanoparticles. *J. Am. Chem. Soc.* **2010**, *132*, 5677–5686. [CrossRef]
102. Li, X.; Li, N.; Zhao, L. The Reactive Activities of Natural Amino Acids: Key Principles of Peptide-Templated Au Cluster Synthesis. *Sci. Bull.* **2016**, *61*, 1732–1738. [CrossRef]
103. Buglak, A.A.; Kononov, A.I. Comparative Study of Gold and Silver Interactions with Amino Acids and Nucleobases. *RSC Adv.* **2020**, *10*, 34149–34160. [CrossRef] [PubMed]
104. Srivastava, R. Interaction of Cysteine with Au_n (n = 8, 10, 12) Even Neutral Clusters: A Theoretical Study. *ChemistrySelect* **2017**, *2*, 2789–2796. [CrossRef]
105. Goel, S.; Velizhanin, K.A.; Piryatinski, A.; Ivanov, S.A.; Tretiak, S. Ligand Effects on Optical Properties of Small Gold Clusters: A TDDFT Study. *J. Phys. Chem. C* **2012**, *116*, 3242–3249. [CrossRef]
106. Akola, J.; Walter, M.; Whetten, R.L.; Häkkinen, H.; Grönbeck, H. On the Structure of Thiolate-Protected Au_{25}. *J. Am. Chem. Soc.* **2008**, *130*, 3756–3757. [CrossRef]
107. Wu, Z.; Jin, R. On the Ligand's Role in the Fluorescence of Gold Nanoclusters. *Nano Lett.* **2010**, *10*, 2568–2573. [CrossRef]
108. Pei, Y.; Zeng, X.C. Investigating the Structural Evolution of Thiolate Protected Gold Clusters from First-Principles. *Nanoscale* **2012**, *4*, 4054. [CrossRef]
109. Chaudhari, K.; Xavier, P.L.; Pradeep, T. Understanding the Evolution of Luminescent Gold Quantum Clusters in Protein Templates. *ACS Nano* **2011**, *5*, 8816–8827. [CrossRef]
110. Liu, Y.; Ai, K.; Cheng, X.; Huo, L.; Lu, L. Gold-Nanocluster-Based Fluorescent Sensors for Highly Sensitive and Selective Detection of Cyanide in Water. *Adv. Funct. Mater.* **2010**, *20*, 951–956. [CrossRef]
111. Peng, J.; Wang, L.; Wang, P.; Pei, Y. Density Functional Theory Computation and Machine Learning Studies of Interaction between Au_3 Clusters and 20 Natural Amino Acid Molecules. *ACS Omega* **2023**, *8*, 23024–23031. [CrossRef]
112. Abdalmoneam, M.H.; Waters, K.; Saikia, N.; Pandey, R. Amino-Acid-Conjugated Gold Clusters: Interaction of Alanine and Tryptophan with Au_8 and Au_{20}. *J. Phys. Chem. C* **2017**, *121*, 25585–25593. [CrossRef]
113. Wang, Y.; Cui, Y.; Zhao, Y.; Liu, R.; Sun, Z.; Li, W.; Gao, X. Bifunctional Peptides That Precisely Biomineralize Au Clusters and Specifically Stain Cell Nuclei. *Chem. Commun.* **2012**, *48*, 871–873. [CrossRef]
114. Song, W.; Wang, Y.; Liang, R.-P.; Zhang, L.; Qiu, J.-D. Label-Free Fluorescence Assay for Protein Kinase Based on Peptide Biomineralized Gold Nanoclusters as Signal Sensing Probe. *Biosens. Bioelectron.* **2015**, *64*, 234–240. [CrossRef] [PubMed]
115. Yuan, M.; Lian, J.; Han, X.; Wen, J.; Gao, J.; Wang, L.; Zhang, F. Real-Time Fluorescence Dynamics in One-Step Synthesis of Gold Nanoclusters Coupling with Peptide Motifs. *Colloids Surf. B Biointerfaces* **2022**, *219*, 112820. [CrossRef] [PubMed]
116. Lopez-Martinez, E.; Gianolio, D.; Garcia-Orrit, S.; Vega-Mayoral, V.; Cabanillas-Gonzalez, J.; Sanchez-Cano, C.; Cortajarena, A.L. Tuning the Optical Properties of Au Nanoclusters by Designed Proteins. *Adv. Opt. Mater.* **2022**, *10*, 2101332. [CrossRef]

117. Feng, J.; Pandey, R.B.; Berry, R.J.; Farmer, B.L.; Naik, R.R.; Heinz, H. Adsorption Mechanism of Single Amino Acid and Surfactant Molecules to Au {111} Surfaces in Aqueous Solution: Design Rules for Metal-Binding Molecules. *Soft Matter* **2011**, *7*, 2113. [CrossRef]
118. Abdalmoneam, M.H.; Saikia, N.; Abd El-Mageed, H.R.; Pandey, R. First Principles Study of the Optical Response of Au $_8$ Cluster Conjugated with Methionine, Tryptophan, and Tryptophyl-methionine Dipeptide. *J Phys. Org. Chem* **2021**, *34*, e4201. [CrossRef]
119. Londoño-Larrea, P.; Vanegas, J.P.; Cuaran-Acosta, D.; Zaballos-García, E.; Pérez-Prieto, J. Water-Soluble Naked Gold Nanoclusters Are Not Luminescent. *Chem. A Eur. J* **2017**, *23*, 8137–8141. [CrossRef]
120. Zhu, M.; Yao, Q.; Liu, Z.; Zhang, B.; Lin, Y.; Liu, J.; Long, M.; Xie, J. Surface Engineering Assisted Size and Structure Modulation of Gold Nanoclusters by Ionic Liquid Cations. *Angew. Chem. Int. Ed.* **2022**, *61*, e202115647. [CrossRef]
121. Wang, Y.; Wang, Y.; Zhou, F.; Kim, P.; Xia, Y. Protein-Protected Au Clusters as a New Class of Nanoscale Biosensor for Label-Free Fluorescence Detection of Proteases. *Small* **2012**, *8*, 3769–3773. [CrossRef]
122. Li, D.; Liu, Q.; Qi, Q.; Shi, H.; Hsu, E.; Chen, W.; Yuan, W.; Wu, Y.; Lin, S.; Zeng, Y.; et al. Gold Nanoclusters for NIR-II Fluorescence Imaging of Bones. *Small* **2020**, *16*, e2003851. [CrossRef] [PubMed]
123. Ni, S.; Liu, Y.; Tong, S.; Li, S.; Song, X. Emerging NIR-II Luminescent Gold Nanoclusters for In Vivo Bioimaging. *J. Anal. Test.* **2023**, *7*, 260–271. [CrossRef]
124. Chen, Q.; Chen, J.; Yang, Z.; Zhang, L.; Dong, Z.; Liu, Z. NIR-II Light Activated Photodynamic Therapy with Protein-Capped Gold Nanoclusters. *Nano Res.* **2018**, *11*, 5657–5669. [CrossRef]
125. Liu, Z.; Luo, L.; Jin, R. Visible to NIR-II Photoluminescence of Atomically Precise Gold Nanoclusters. *Adv. Mater.* **2023**, *36*, e2309073. [CrossRef]
126. Song, X.; Zhu, W.; Ge, X.; Li, R.; Li, S.; Chen, X.; Song, J.; Xie, J.; Chen, X.; Yang, H. A New Class of NIR-II Gold Nanocluster-Based Protein Biolabels for In Vivo Tumor-Targeted Imaging. *Angew. Chem. Int. Ed.* **2021**, *60*, 1306–1312. [CrossRef]
127. 'Bertorelle, F.; Wegner, K.D.; Perić Bakulić, M.; Fakhouri, H.; Comby-Zerbino, C.; Sagar, A.; Bernadó, P.; Resch-Genger, U.; Bonačić-Koutecký, V.; Le Guével, X.; et al. Tailoring the NIR-II Photoluminescence of Single Thiolated Au_{25} Nanoclusters by Selective Binding to Proteins. *Chem. A Eur. J* **2022**, *28*, e202200570. [CrossRef]
128. Zhang, X.-D.; Wu, D.; Shen, X.; Liu, P.-X.; Fan, F.-Y.; Fan, S.-J. In Vivo Renal Clearance, Biodistribution, Toxicity of Gold Nanoclusters. *Biomaterials* **2012**, *33*, 4628–4638. [CrossRef]
129. Xu, J.; Yu, M.; Peng, C.; Carter, P.; Tian, J.; Ning, X.; Zhou, Q.; Tu, Q.; Zhang, G.; Dao, A.; et al. Dose Dependencies and Biocompatibility of Renal Clearable Gold Nanoparticles: From Mice to Non-human Primates. *Angew. Chem. Int. Ed.* **2018**, *57*, 266–271. [CrossRef]
130. Liu, H.; Hong, G.; Luo, Z.; Chen, J.; Chang, J.; Gong, M.; He, H.; Yang, J.; Yuan, X.; Li, L.; et al. Atomic-Precision Gold Clusters for NIR-II Imaging. *Adv. Mater.* **2019**, *31*, 1901015. [CrossRef]
131. Liu, H.; Li, Y.; Sun, S.; Xin, Q.; Liu, S.; Mu, X.; Yuan, X.; Chen, K.; Wang, H.; Varga, K.; et al. Catalytically Potent and Selective Clusterzymes for Modulation of Neuroinflammation through Single-Atom Substitutions. *Nat. Commun.* **2021**, *12*, 114. [CrossRef]
132. Guo, M.; Zhang, G.; Zhao, R.; Ma, H.; Yan, Y.; Yang, S.; Meng, J.; Huang, Y.; Zhang, X.-D.; Wang, H.; et al. Ligand Engineering of Gold Nanoclusters for NIR-II Imaging. *ACS Appl. Nano Mater.* **2023**, *6*, 15945–15958. [CrossRef]
133. Ma, H.; Zhang, X.; Liu, L.; Huang, Y.; Sun, S.; Chen, K.; Xin, Q.; Liu, P.; Yan, Y.; Wang, Y.; et al. Bioactive NIR-II Gold Clusters for Three-Dimensional Imaging and Acute Inflammation Inhibition. *Sci. Adv.* **2023**, *9*, eadh7828. [CrossRef] [PubMed]
134. Gao, P.; Wu, S.; Chang, X.; Liu, F.; Zhang, T.; Wang, B.; Zhang, K.-Q. Aprotinin Encapsulated Gold Nanoclusters: A Fluorescent Bioprobe with Dynamic Nuclear Targeting and Selective Detection of Trypsin and Heavy Metal. *Bioconjug. Chem.* **2018**, *29*, 4140–4148. [CrossRef] [PubMed]
135. Xie, J.; Zheng, Y.; Ying, J.Y. Highly Selective and Ultrasensitive Detection of Hg^{2+} Based on Fluorescence Quenching of Au Nanoclusters by Hg^{2+}–Au+ Interactions. *Chem. Commun.* **2010**, *46*, 961–963. [CrossRef] [PubMed]
136. Selvaprakash, K.; Chen, Y.C. Using protein-encapsulated gold nanoclusters as photoluminescent sensing probes for biomolecules. *Biosens. Bioelectron.* **2014**, *61*, 88–94. [CrossRef]
137. Nain, A.; Tseng, Y.-T.; Lin, Y.-S.; Wei, S.-C.; Mandal, R.P.; Unnikrishnan, B.; Huang, C.-C.; Tseng, F.-G.; Chang, H.-T. Tuning the Photoluminescence of Metal Nanoclusters for Selective Detection of Multiple Heavy Metal Ions. *Sens. Actuators B Chem.* **2020**, *321*, 128539. [CrossRef]
138. Zang, J.; Li, C.; Zhou, K.; Dong, H.; Chen, B.; Wang, F.; Zhao, G. Nanomolar Hg $^{2+}$ Detection Using β-Lactoglobulin-Stabilized Fluorescent Gold Nanoclusters in Beverage and Biological Media. *Anal. Chem.* **2016**, *88*, 10275–10283. [CrossRef]
139. Raju, S.; Manalel Joseph, M.; Kuttanpillai, R.P.; Padinjarathil, H.; Gopalakrishnan Nair Usha, P.; Therakathinal Thankappan Nair, S. Polysaccharide Enabled Biogenic Fabrication of pH Sensing Fluorescent Gold Nanoclusters as a Biocompatible Tumor Imaging Probe. *Microchim. Acta* **2020**, *187*, 246. [CrossRef]
140. Dutta, D.; Sailapu, S.K.; Simon, A.T.; Ghosh, S.S.; Chattopadhyay, A. Gold-Nanocluster-Embedded Mucin Nanoparticles for Photodynamic Therapy and Bioimaging. *Langmuir* **2019**, *35*, 10475–10483. [CrossRef]

141. Poderys, V.; Jarockyte, G.; Bagdonas, S.; Karabanovas, V.; Rotomskis, R. Protein-Stabilized Gold Nanoclusters for PDT: ROS and Singlet Oxygen Generation. *J. Photochem. Photobiol. B Biol.* **2020**, *204*, 111802. [CrossRef]
142. Chakraborty, I.; Pradeep, T. Atomically Precise Clusters of Noble Metals: Emerging Link between Atoms and Nanoparticles. *Chem. Rev.* **2017**, *117*, 8208–8271. [CrossRef] [PubMed]
143. Chevrier, D.M. Properties and Applications of Protein-Stabilized Fluorescent Gold Nanoclusters: Short Review. *J. Nanophoton* **2012**, *6*, 064504. [CrossRef]
144. Qian, S.; Wang, Z.; Zuo, Z.; Wang, X.; Wang, Q.; Yuan, X. Engineering Luminescent Metal Nanoclusters for Sensing Applications. *Coord. Chem. Rev.* **2022**, *451*, 214268. [CrossRef]
145. Antoine, R.; Maysinger, D.; Sancey, L.; Bonačić-Koutecký, V. Open Questions on Proteins Interacting with Nanoclusters. *Commun. Chem.* **2022**, *5*, 47. [CrossRef]